Atmos. Chem. Phys. Discuss., https://doi.org/10.5194/acp-2018-194
Manuscript under review for journal Atmos. Chem. Phys.
Discussion started: 5 April 2018

Atmospheric Chemistry and Physics Discussions

Cloud vertical structure over a tropical station obtained using long-term high resolution Radiosonde measurements

Nelli Narendra Reddy, Madineni Venkat Ratnam*, Ghouse Basha and Varaha Ravikiran

National Atmospheric Research Laboratory, Department of Space, Gadanki-517112, India.

*vratnam@narl.gov.in

Abstract

Cloud vertical structure, including top and base altitudes, thickness of cloud layers, and the vertical distribution of multi-layer clouds affects the large-scale atmosphere circulation by altering gradients in the total diabatic heating/cooling and latent heat release. In this study, long-term (11 years) observations of high vertical resolution radiosondes are used to obtain the cloud vertical structure over a tropical station, Gadanki (13.5^{o} N, 79.2^{o} E), India. The detected cloud layers are verified with independent observations using cloud particle sensor (CPS) sonde launched from the same station. High-level clouds account for 69.05%, 58.49%, 55.5%, and 58.6% of all clouds during pre-monsoon, monsoon, post-monsoon, and winter seasons, respectively. The average cloud base (cloud top) altitude for low-level, middle-level, high-level and deep convective clouds are 1.74 km (3.16 km), 3.59 km (5.55 km), 8.79 km (10.49 km), and 1.22 km (11.45 km), respectively. Single-layer, two-layer, and three-layer clouds account for 40.80%, 30.71%, and 19.68% of all cloud configurations, respectively. Multi-layer clouds occurred more frequently during the monsoon with 34.58%. Maximum cloud top altitude and the cloud thickness occurred during monsoon season for single-layer clouds and the uppermost layer of multiple layer cloud configurations. In multi-layer cloud configurations, diurnal variations in the thickness of upper layer clouds are larger than those of lower layer clouds. Heating/cooling in the troposphere and lower stratosphere due to these clouds layers is also investigated and found peak cooling (peak warming) below (above) the Cold Point Tropopause (CPT) altitude. The magnitude of cooling (warming)

increases from single-layer to four or more-layer cloud occurrence. Further, the vertical structure of clouds is also studied with respect to the arrival date of Indian summer monsoon over Gadanki.

Keywords: Cloud vertical structure, Single-layer clouds, Multi-layer clouds, Cloud base, top and thickness

1. Introduction

Clouds are vital in driving the climate system as they play important role in radiation budget, general circulation and hydrological cycle (Ramanathan et al., 1989; Rossow and Lacis, 1990; Wielicki et al., 1995; Li et al., 1995; Stephens, 2005; Yangetal., 2010; Huang,2013). By interacting with both shortwave and long-wave radiation, clouds play crucial role in the radiative budget at the surface, within and at the top of the atmosphere (Li et al., 2011; Ravi Kiran et al., 2015; George et al., 2018). Clouds and the general circulation of Earth's atmosphere are linked in an intimate feedback loop. Clouds result from the water vapor transports and cooling by atmospheric motions. The forcing for the atmospheric circulation is significantly modified by vertical and horizontal gradients in the radiative and latent heat fluxes induced by the clouds (Chahine et al., 2006 and Li et al., 2005). The complexity of the processes involved, the vast amount of information needed, including vertical and spatial distribution, and the uncertainty associated with the available data, all add difficulties to determine how clouds contribute to climate change (e.g., Heintzenberg and Charlson, 2009). In particular, knowledge about cloud type is very important, because the overall impact of clouds on the Earth's energy budget is difficult to estimate, as it involves two opposite effects depending on cloud type (Naud et al., 2003). Low, highly reflective clouds tend to cool the surface, whereas high, semi-transparent clouds tend to warm it, because they let much of the shortwave radiation through but are opaque to the long-wave radiation. Whereas deep convective clouds (DCCs) neither warm nor cool the surface,

because their cloud greenhouse and albedo forcing's nearly balance. However, DCCs produce fast vertical transport, redistributing water vapour and chemical constituents and influence the thermal structure of the Upper Troposphere and Lower Stratosphere (UTLS) (Biondi et al., 2012).

Changes in the cloud vertical structure (locations of cloud top and base, number and thickness of cloud layers) affect the atmospheric circulations by modifying the distribution of radiative and latent heating rates within the atmosphere (e.g., Slingo and Slingo, 1988; Randall et al., 1989; Slingo and Slingo, 1991; Wang and Rossow, 1998; Li et al., 2005 and Chahine et al., 2006; Cesana and Chepfer, 2012; Rossow and Zhang, 2010; Rossow et al., 2005; Wang et al., 2014b). The effects of cloud vertical structure (CVS) on atmospheric circulation have been described using atmospheric models by many authors. Crewell et al. (2004) underlined the importance of clouds in multiple scattering and absorption of sunlight, processes that have a significant impact on the diabatic heating in the atmosphere. The vertical gradients in the cloud distribution were somewhat more important to the circulation strength than horizontal gradients (Rind and Rossow, 1984). These complex phenomena are not yet fully understood and are subject to large uncertainties. In fact, the assumed or computed vertical structure of cloud occurrence in general circulation models (GCMs) is one of the main reasons why different models predict a wide range of future climates. For example, most GCMs underestimate the cloud cover, while only a few overestimate it (Xi et al., 2010). Therefore, to improve the understanding of cloud-related processes, and then to increase the predictive capabilities of large-scale models (including global circulation models), better and more accurate observations of CVSis needed. The present work is a contribution towards addressing this need.

Ground-based instruments (e.g. Warren et al., 1988; Hahn et al., 2001), active sensor satellites (e.g.Stephens et al., 2008; Winker et al., 2007) and upper air measurements from

radiosondes (Wang et al., 2000) are usually applied to observe and describe the CVS. Ground-based instruments such as lidar, cloud radar and ceilometers provide cloud measurements with continuous temporal coverage; Lidars and ceilometers are very efficient at detecting clouds and can locate the bottom of cloud layer precisely, but cannot usually detect the cloud top, due to attenuation of the beam within the cloud. The vertically pointing cloud radar is able to detect the cloud top, although signal artifacts can cause difficulties during precipitation (Nowak et al., 2008).On the other hand, passive sensor satellite data, such as from ISCCP (the International Satellite Cloud Climatology Project) and MODIS (the Moderate Resolution Imaging Spectroradiometer), do exist limitations. For example, the thin clouds are indistinguishable from aerosols in ISCCP when optical thickness is less than 0.3–0.5) (Rossow and Garder, 1993); Both ISCCP and MODIS underestimate low-level clouds and overestimate middle-level cloud (Li et al., 2006; Naud and Chen, 2010). Hence, conventional passive-sensor satellite data, largely miss the comprehensive information on the vertical distribution of cloud layers.

The precipitation radar and TRMM Microwave Imager on-board the Tropical Rainfall Measuring Mission (TRMM) satellite are helpless in observing small-size particles despite of its capability of penetrating rainy cloud and obtaining the internal three-dimensional information, and only larger rainfall particles can be observed due to limitations of its working broadband. On the other hand, active sensors such as the Cloud Profiling Radar (CPR) on CloudSat and the Cloud-Aerosol Lidar with Orthogonal Polarization (CALIOP) aboard CALIPSO (Cloud Aerosol Lidar and Infrared Pathfinder Satellite Observation) satellites are achieving notable results by including a vertical dimension to traditional satellite images. CPR is a 94GHz nadir-looking radar which is able to penetrate the optically thick clouds, while CALIOP is able to detect tenuous cloud layer that are below the detection threshold of radar. In other words, it has the ability to detect shallow clouds. Therefore,

accurate location of cloud top and complete vertical structure information of cloud can be obtained by the combined use of CPR and CALIOP, because of their unique complementary skills. Previous researches have shown that CloudSat/CALIPSO data are credible compared with ISCCP and ground observation data (Sassen and Wang, 2008; Naud and Chen, 2010; Kim et al., 2011; Noh et al., 2011; Jiang et al., 2011). However, because the repeat time of these polar orbiting satellites for any particular location is very large, the time resolution of such observations is low (L'Ecuyer and Jiang, 2010; Qian et al., 2012). Both ground-based and space-based measurements have the problem of overlapping cloud layers that hide each other.

For completeness here we listed other techniques which have been developed for detecting cloud top heights from passive sensors. The CO_2-slicing method uses CO_2 differential absorption in the thermal infrared spectral range (Rossow and Schiffer, 1991; King et al., 1992; Platnick et al., 2003). Ultraviolet radiances can also be used as rotational Raman scattering causes depletion or filling of solar Fraunhofer lines in the UV spectrum, depending on the Rayleigh scattering above the cloud (Joiner and Bhartia, 1995; de Beek et al., 2001). Similarly, the polarization of reflected light, at visible shorter wavelength, due to Rayleigh scattering carries information on cloud top height (Goloub et al., 1994; Knibbe et al., 2000). Finally, cloud top height can also be retrieved by applying geometrical methods to stereo observations (Moroney et al., 2002; Seiz et al., 2007; Wu et al., 2009). Global Navigation Satellite System (GNSS) Radio Occultation (RO) profiles were used to detect the convective cloud top heights (Biondi et al., 2013). Recently, Biondi et al. (2017) used GNSS RO profiles to detect the top altitude of volcanic clouds and analyzed their impact on thermal structure of Upper Troposphere and Lower Stratosphere. Multi-angle and bi-spectral measurements in the O_2 A-band were used to derive the cloud top altitude and cloud geometrical thickness (Merlin et al., 2016 and references therein). However, this method is

restricted to homogeneous plane-parallel clouds. For heterogeneous clouds or when aerosols lay above the clouds the spectra of reflected sunlight in the O_2 A-band will get modified.

An indirect way to perform estimations of CVS is by using atmospheric thermodynamic profiles as measured by radiosondes. Radiosondes can penetrate atmospheric (and cloud) layers to provide in situ data. The profiles of temperature, relative humidity and pressure measured by radiosondes provide information about the CVS by identifying saturated levels in the atmosphere (Zhang et al., 2010). In fact, radiosonde measurements were probably the best measurements for obtaining the CVS from the ground (Wang et al., 2000; Eresmaa et al., 2006; Zhang et al., 2010). Very recently, George et al. (2018) provided CVS over India during depression (D) and non-depression (ND) events during South West monsoon season (July 2016) using one month of campaign data. However, detailed CVS in all the seasons including diurnal variation over Indian region is not made so far to the best of our knowledge.

Our main objective is to examine the temperature structure of UTLS region during the occurrence of single-layer and multi-layer clouds over Gadanki location (13.5^o N, 79.2^o E). In the first, we focus to report the CVS using long-term (11 years) high vertical resolution radiosondes observations. The paper is organized as follows: data and methodology are described in section 2. In section 3, background weather conditions during the period of analysis are described. Results and discussion are given in section 4. Finally, the summary and major conclusion drawn from the present study is provided in section 5.

2. Data and Methodology

2.1. Data

In this study, long-term (11 years) observations of high vertical resolution radiosonde (Väisälä RS-80, RS-92; Meisei RS-01GII,RS-6G, RS-11G, IMS-100) data is used to analyze CVS over a tropical station, Gadanki.There is no significant change in the accuracies of the meteorological parameters from these different radiosonde makes. Most of these radiosondes

were launched around 1730 Local Time, LT (LT=UT+0530 h). Figure 1 shows the monthly percentage of radiosonde data available during Apr. 2006 to May 2017. Total 3313 launches were made, out of which 98.9% and 86.6% reached altitudes greater than 12.5 km and 20 km, respectively. The data which have balloon burst altitude less than 12.5 km (1.1%) are discarded. Also, we have put condition that the number of profiles in a month should be more than seven to represent that month. After applying these two conditions the total number of profiles came to 3251. In addition, to study the diurnal variations in CVS over Gadanki, we made use of radiosonde observations taken from Tropical Tropopause Dynamics (TTD) campaigns (Venkat Ratnam et al., 2014b) conducted during Climate and Weather of Sun Earth Systems (CAWSES) India Phase II program (Pallamraju et al., 2014). During these campaigns, the radiosondes were launched every three hourly for 72 hour in each month during Dec. 2010 to Mar.2014 except in Dec. 2012, Jan., Feb., Apr., 2013.

2.2. Methodology

There are several methods available in the literature to determine the CVS from the profiles of radiosonde data (Poore et al., 1995; Wang and Rossow, 1995; Chernykh and Eskridge, 1996; Minnis et al., 2005; Zhang et al., 2010). Poore et al. (1995) estimated the cloud base and cloud top using temperature-dependent dew-point depression thresholds. First, the dew-point depression must be calculated at every radiosonde level. According to Poore et al. (1995), a given atmospheric level has a cloud if $\Delta T_d < 1.7\ ^oC$ at $T > 0\ ^oC$, $\Delta T_d < 3.4\ ^oC$ at $0 > T > -20^oC$, $\Delta T_d < 5.2^oC$ at $T < -20^oC$.

Wang and Rossow (1995) used the temperature, pressure and RH profiles and computed RH with respect to ice instead of liquid water for levels with temperatures lower than 0 ^oC. To this new RH profile they have applied two RH thresholds (min RH = 84% and max RH = 87%).In addition, if RH at the base (top) of the moist layer is lower than 84%, a RH jump exceeding 3% must exist from the underlying (above) level. According to the Chernykh and

Eskridge (1996) method, the necessary condition for the existence of clouds in a given atmospheric level is that the second derivatives with respect to height (z) of temperature and RH to be positive and negative, respectively ie., $T''(z) \geq 0$ and $RH''(z) \leq 0$. Minnis et al. (2005) provided an empirical parameterization that calculates the probability of occurrence of a cloud layer using RH and air temperature from radiosondes. First, RH values must be converted to RH with respect to ice when temperature is less than −20 ^{o}C; on the other hand, the profile has to be interpolated every 25 hPa up to the height of 100 hPa. An expression to estimate the cloud probability (Pcld) as a function of temperature and RH is then applied; in this formula, where RH is given the maximum influence as it is the most important factor in cloud formation. Finally, a cloud layer is set wherever Pcld ≥ 67%.The Zhang et al. (2010) method is an improvement on the Wang and Rossow (1995) method. Instead of a single RH threshold, Zhang et al. (2010) applied altitude-dependent thresholds without the requirement of the 3% RH jump at the cloud base and top.

Costa-Suros et al. (2014) compared the CVS derived from these five methods described above by using 193 radiosonde profiles acquired at the Atmospheric Radiation Measurement (ARM) Southern Great Plains site during all seasons of the year 2009. The performance of the five methods has been assessed by comparing with Active Remote Sensing of Clouds (ARSCL) data taken as a reference. Costa-Suros et al. (2014) concluded that three of the methods (Poore et al., 1995; Wang and Rossow, 1995; and Zhang et al., 2010) perform reasonably well, giving perfect agreements for 50% of the cases and approximate agreements for 30% of the cases. The other methods gave poorer results (lower perfect and/or approximate agreement, and higher false positive, false negative or not coincident detections). Among the three methods, Zhang et al. (2010) method is the most recent version of the treatment initially proposed in Poore et al. (1995) and Wang and Rossow (1995), and provides good enough results (a perfect agreement of 53.9% and an approximate agreement

of 29.5%).Thus, the algorithm of Zhang et al. (2010) is used for detecting cloud layers in our analysis and we provide details of Zhang et al. (2010) algorithm.

Cloud layers are associated with high RH values above some threshold as the radiosonde penetrates through them. Cloud detection algorithm of Zhang et al. (2010) employs three height-resolving RH thresholds to determine cloud layers: minimum and maximum RH thresholds in cloud layers (min-RH and max-RH), and minimum RH thresholds within the distance of two contiguous layers (inter-RH).The height-resolving thresholds of max-RH, min-RH, and inter-RH values are specified in Table 1. The algorithm begins by converting RH with respect to liquid water to RH with respect to ice at temperatures below 0^{o} C (see example in Figure 2). The accuracy of RH measurement is less than 5% up to the altitude 12.5 km and hence the RH profile is examined from the surface to the 12.5 km (~ 200 hPa) altitude to find cloud layers in seven steps: (1) the base of the lowest moist layer is determined as the level when RH exceeds the min-RH corresponding to this level; (2) above the base of the moist layer, contiguous levels with RH over the corresponding min-RH are treated as the same layer; (3) the top of the moist layer is identified when RH decreases to that below the corresponding min-RH or RH is over the corresponding min-RH but the top of the profile is reached; (4) moist layers with bases lower than 500 m AGL (Above Ground Level) and thickness less than 400 m are discarded; (5) the moist layer is classified as a cloud layer if the maximum RH within this layer is greater than the corresponding max-RH at the base of this moist layer; (6) two contiguous layers are considered as a one-layer cloud if the distance between these two layers is less than 300 m or the minimum RH within this distance is more than the maximum inter-RH value within this distance; and (7) clouds are discarded if their thicknesses are less than 100 m.

Before proceeding further, it is desired to verify the identified layers of clouds are correct or not with independent observations. For that we have launched Cloud Particle Sensor (CPS)

sonde (Fujiwara et al., 2016) at Gadanki, which provides profile of cloud number concentration. Results from a flight of RS-11G radiosonde and Cloud Particle Sensor (CPS) Sonde on the same balloon launched at 02 LT on 04 Aug. 2017 at Gadanki, India is shown in Figure 2. Sudden increase in the cloud number concentration within the detected cloud layers indicates the cloud layer boundaries detected in the present study are accurate.

The drawback of using the radiosonde data for detecting the CVS at a given location is the radiosonde horizontal displacement, due to the drift produced by the wind. However, irrespective of the season, the maximum horizontal drift of radiosonde when it reaches the 12.5 km altitude is always less than 20 km (Venkat Ratnam et al., 2014a). One may expect different background features within this 20 km particularly the localised convection that may influence the CVS. In order to assess this aspect, we used outgoing longwave radiation (OLR) as a proxy for tropical convection. Figure 3(a-d) describes the seasonal mean distribution of OLR (from KALPANA-1 satellite) around Gadanki location obtained during pre-monsoon, monsoon, post-monsoon and, winter seasons averaged during 2006 – 2017. It can be noted that irrespective of the season, homogeneous cloudiness prevailed for more than 50 km radius around Gadanki location. Hence the CVS detected from the radiosonde can be treated as representative of Gadanki location.

Methodology described in section 2.2 to detect CVS is applied on high vertical resolution radiosonde data acquired during Apr. 2006 to May 2017 from Gadanki, as well as special radiosondes launches during TTD campaigns from Oct. 2010 to Apr. 2014. Results are presented in Section 4. Before going further, it is desirable to examine the background weather conditions prevailing over Gadanki during different seasons.

3. Background weather conditions

National Atmospheric Research Laboratory (NARL) at Gadanki is located about 120km northwest of Chennai (Madras) on the east coast of the southern Indian peninsula. This

station is surrounded by hills with a maximum altitude of 350–400m above the station, and the station is at an altitude of 375ma.m.s.l. (hereinafter all altitudes are mentioned above mean sea level only). The local topography is complex with a number of small hillocks around and a high hill of ~1km about 30km from the balloon launching site in the northeast direction. The detailed topography of Gadanki is shown in Basha and Ratnam (2009). Gadanki receives 53% of the annual rainfall during the southwest monsoon (Jun. to Sep.) and 33% of the annual rainfall during the northeast monsoon (Oct. to Dec.) (Rao et al., 2008a). The rainfall during the southwest monsoon occurs predominantly during the evening to midnight period. About 66% of total rainfall is convective in nature, while the remaining rain is widespread stratiform in character (Rao et al., 2008a).

Background meteorological conditions prevailing over the observational site are briefly described based on the radiosonde data collected during Apr. 2006 to May 2017. The seasons are classified as winter (December-January- February), pre-monsoon (March-April-May), monsoon (June-July-August-September), post-monsoon (October-November). The climatological monthly mean contours of the temperature anomalies, relative humidity, zonal and meridional winds are shown in Figure4a–d, respectively. From surface to 1 km altitude, temperature shows seasonal variability with warmer temperatures during pre-monsoon months and relatively cooler temperatures during winter season (Figure 4a). Temperature does not show significant variations seasonally from 1 km altitude to the middle troposphere, but shows variations in the lower stratosphere. There exist significant seasonal variations in the RH (Figure 4b). During winter, RH is small (40 – 50%) from surface to ~ 3 km altitude and is almost negligible above. However, during the other seasons, particularly in the peak monsoon months (Jul. and Aug.), large RH values (60–70%) are noticed up to 10 km altitude.

During winter, easterlies exist up to 4–6 km altitude and westerlies above (Figure 4c). There seem to be weak easterlies above the altitude of 14km during the pre-monsoon. During

the monsoon season low level westerlies exist below 7–8km and easterlies above. The Tropical Easterly Jet (TEJ) is prevalent over this region in the SW monsoon season, with peak velocity sometimes reaching more than 40ms^{-1} (Roja Raman et al., 2009). There exist large vertical shears during monsoon in the zonal wind. Easterlies exist up to 20 km altitude during post-monsoon season. In general, meridional velocities are very small and are northerlies up to 8km and southerlies above in all the seasons, except during monsoon (Figure 4d). During the winter and monsoon, relatively stronger southerlies and northerlies prevailed, respectively, between 12 to 15 km altitudes. A clear annual oscillation can be noticed in both zonal and meridional velocities. Similar variations are also observed by the MST radar located at the same site in between 4 and 20km (Ratnam et al., 2008; Basha and Ratnam, 2009; Debashis Nath et al., 2009). Monthly mean OLR around Gadanki at 1730 LT is shown in Figure 4e. Low values of OLR (< 220 W m^{-2}) around Gadanki location indicate that the occurrence of very deep convection during the monsoon season, consistent with the occurrence of high RH values up to 10 km altitude during monsoon season (Figure 4b).

4. Results

By adopting the methodology described in section 2.2 we have detected a total of 4309 Cloud layers from 3251 radiosonde launches at Gadanki location during the period of data analysis. For each season, cloud layers during Apr. 2006 – May 2017 are averaged to obtain the composite picture of CVS. Seasonal variability in cloud layers is discussed in section 4.2.

4.1. Diurnal variation of single-layer and multi-layer clouds

There are studies on the diurnal variation of cloud layers outside the Indian region. For example, over Porto Santo Island during the Atlantic Stratocumulus Transition Experiment (ASTEX) by Wang et al. (1999), over San Nicolas Island during First ISCCP Regional Experiment (FIRE) by Blaskovic et al. (1990), Over Shouxian (32.56^{o} N, 116.78^{o} E) location by Zhang et al. (2010). As per authors knowledge there are no studies on diurnal variability

of cloud layers over Indian region. For the first time, over Indian land region, the diurnal variability of cloud layers are studied by using radiosonde observations taken from TTD campaigns. Figure 5(a-d) describes the diurnal variations of single-layer and multi-layer clouds during pre-monsoon, monsoon, post-monsoon, and winter seasons over Gadanki region. As mentioned in section 2.1, from Oct. 2010 to Apr.2014, we have launched radiosondes every three hourly for continuous three days in every month except during Nov. 2010. The total number of profiles taken during pre-monsoon, monsoon, post-monsoon, and winter seasons are 160, 254, 101, and 199, respectively. Among these the number of cloudy profiles are 93 in pre-monsoon, 241 in monsoon, 63 in post-monsoon, and 96 in winter seasons.

From the Figure 5(a-d), for four seasons, diurnal variations of cloud occurrence show a maximum between 23 to 05 LT and a minimum at 14 LT, except during monsoon season. During which, a minimum in cloud occurrence occurred at 11 LT. Using Infrared Brightness temperature data over Indian region Gambheer and Bhat (2001), Zuidema (2003), Reddy and Rao (2018) observed the maximum frequency of occurrence of clouds during late night early morning hours. Percentage occurrence of one-layer and multi-layer clouds shows noticeable diurnal variations in all seasons except in monsoon season. Maximum percentage occurrence in one-layer clouds is at 08 LT in pre-monsoon season and it is at 17 LT during post-monsoon and winter seasons. For all the seasons, the maximum percentage occurrence in multi-layer clouds is between 20 to 05 LT.Figure 6(a-d) describe the mean vertical locations (base and top) and cloud thicknesses of one-layer clouds during pre-monsoon, monsoon, post-monsoon, and winter seasons, respectively. During monsoon season, the maximum in cloud top altitude is at 05 LT and minimum is at 14 LT (Figure 6(b)). In general, cloud base of one-layer cloud occur at higher altitude between 11 – 14 LT and it occur relatively low altitudes between 20 – 08 LT. Except during post-monsoon season, the single-layer clouds

326 are high-level clouds with base is greater than 5 km most of the times. During post-monsoon
327 season, the single-layer clouds are low-level at 05 LT (cloud-base altitude of 1.4 km) and
328 middle level-clouds between 14 – 02 LT (Figure 6c). During pre-monsoon and monsoon
329 seasons, thickness of single-layer clouds reaching a maximum at 23 LT and a minimum at 14
330 LT (Figure 6(a-b)). The minimum in one-layer cloud thickness at 14 LT is due to the increase
331 of cloud base altitude and simultaneous decrease of cloud top altitude. There is not much
332 variability in thickness of one-layer clouds during post-monsoon and winter seasons (Figure
333 6(c-d)). Figure 7(a-d) and Figure S1(a-d) are same as Figure 6(a-d) but for two-layer and
334 three-layer clouds. Similar to one-layer cloud, the cloud base of bottom-layer of two-layer
335 clouds show maximum between 11 – 14 LT and minimum between 20 – 08 LT. Thickness of
336 top layer and bottom layer of two-layer clouds reaching a minimum value between 11 – 14
337 LT. Upper layer of two–layer clouds show a maximum in thickness at 23 LT and minimum at
338 11 LT during monsoon season (Figure 7(b)).

339 The cloud maintenance and development are strongly modulated by adiabatic processes,
340 namely solar heating and longwave (LW) radiative cooling (Zhang et al., 2010).Near
341 noontime (11 - 14 LT), solar heating is so strong that (1) evaporation of cloud drops may
342 occur and (2) atmospheric stability may increase thus suppressing cloud development. So
343 near noontime, the vertical development of single-layer clouds and the vertical development
344 of the uppermost layer of multiple layers of cloud are suppressed due to solar heating. This
345 effect is predominant during monsoon season for one-layer and two-layer clouds (Figures
346 6(b) and 7(b)), during pre-monsoon and post-monsoon seasons for three-layer clouds (Figures
347 S1a and S1c). However, for lower layers of cloud in a multiple-layer cloud configuration,
348 solar heating is greatly reduced because of the absorption and scattering processes of the
349 upper layers of cloud. In general maximum in surface temperature occurs around 15:20 LT
350 (Reddy and Rao, 2018). The ground surface is warmer than any cloud layer so through the

exchange of LW radiation, the cloud base gains more energy. This facilitates cloud development and leads to a maximum in cloud altitude and thickness between 14 – 17 LT (Figures 7a, 7b, 7d and S1a). This effect is predominant during winter season for two layer clouds (Figure 7d) and during pre-monsoon season for three-layer clouds (Figure S1a). As the sun sets, LW radiative cooling starts to dominate over shortwave (SW) radiative warming. Cloud top temperatures begin to lower, which increases atmospheric instability and fuels the development of single-layer clouds and the uppermost layer of cloud in multiple-layer cloud configurations. At sunset, solar heating diminishes and LW cooling strengthens, which may explain why there is a peak between 20 – 23 LT in the thickness of one-layer clouds and the uppermost layer of two-layer cloud. This effect is clearly observed in the monsoon season (Figures 6b, 7b, S1b). We conclude that diurnal variability in base, top and thickness for single-layer, two-layer and, three-layer clouds are significant. Hence there can be a bias in cloud vertical structure when we are studying the composite over a season by using polar satellites.

Next section, we show the seasonal variability in cloud layers using long-term (11 years) observations of high vertical resolution radiosonde over Gadanki. Note that most of these radiosondes were launched around 1730 LT hence there will be bias in the results due to diurnal variability of cloud layers which we have discussed above. Hence the results related to seasonal variability of cloud layers are only representative of 1730 LT.

4.2. Seasonal variability in the cloud layers

Figure 8(a-c) describe the percentage occurrence of base, top and thickness of cloud layers observed during different seasons over Gadanki. The cloud base altitude shows a bimodal distribution in all seasons except during pre-monsoon season (Figure 8a). During pre-monsoon season, the peak of cloud base altitude distribution is observed at ~6.2 km (~7.5%). During other three seasons (monsoon, post-monsoon and winter), the first peak in

cloud base altitude is observed between 2 and 3 km altitude region and the second peak is observed at ~6.2 km. Using CLOUDSAT observations over the Indian monsoon region, Das et al. (2017) also reported that the cloud base altitude over Indian monsoon region shows a bimodal distribution. However, the first peak in cloud base altitude is observed at ~14 km while the second maximum is at 2 km.

The cloud top altitude increases above 12 km altitude and have a maximum at 12.5 km in all seasons (Figure 8b). Note that we restrict maximum altitude as 12.5 km due to limitation in providing reliable water vapour above that altitude from normal radiosondes. At lower altitudes, during the monsoon season the peak in cloud top altitude is at 2.9 km and it increases to 3.3 km during the post-monsoon season. However we have also checked the CVS till 18 km. There is no significant difference in the cloud base and cloud top altitude distribution (See Figure S2). Das et al. (2017) reported that there are two peaks in the cloud top altitude; one at ~17 km and other is at ~3 km. The peaks in cloud base and cloud top at higher altitudes as observed by Das et al. (2017) could be due to the occurrence of cirrus clouds.

The cloud base altitude values are subtracted from the cloud top altitude for each cloud layer to extract the cloud thickness. Figure 8(c) describes the percentage occurrence of the cloud thickness observed during different seasons. The occurrence of thicker clouds decreases exponentially. The cloud thickness has a maximum below 500 m for all seasons, which constituted about 34.7%, 26.5%, 31.2% and 36.6% of the total observed cloud layers during pre-monsoon, monsoon, post-monsoon and winter seasons, respectively. In general, for all seasons, more than 65% of clouds layers have cloud thickness < 2 km.

Different cloud types occurring at different height regions have a spectrum of effects on the radiation budget (Behrangi et al., 2012). Therefore, the clouds have been classified into four groups based on the cloud base altitude and their thickness (Lazarus et al., 2000 and

Zhang et al., 2010): (1) low-level clouds with bases lower than 2 km and thickness less than 6 km; (2) middle-level clouds with bases ranging from 2 to 5 km; (3) high-level clouds with bases greater than 5 km; and (4) deep convective cloud (hereafter called DCC) with bases less than 2 km and thicknesses greater than 6 km. These four types of clouds account for 11.97%, 26.71%, 59.36% and 1.95% of all cloudy cases, respectively. Figure 9(a-d) describe the mean vertical locations (base and top), cloud thicknesses and percentage occurrence of low-, middle-, high-level clouds, and DCC observed during different seasons. At Gadanki location, there is a distinct persistence of the high-level clouds over all the seasons. The occurrence of the high-level clouds is 69.05%, 58.49%, 55.5%, 58.6% during the pre-monsoon, monsoon, post-monsoon, and winter seasons, respectively (Figure 9c). Zuidema (2003) reported that the deep convective systems generated over central and west BoB advect toward the inland region of southern peninsular India and dissipates. The outflow caused by the deep convective systems could be responsible for the higher percentage occurrence of high-level clouds. The low-level (middle-level) clouds contribute about 3.74%, 10.45%, 16.27%, and 20.89% (27.04%, 29.35%, 24.28%, and 18.67%) of all cloudy cases during the pre-monsoon, monsoon, post-monsoon, and winter seasons, respectively (Figure 9a-b).

Thicknesses of low-, middle-, high-level clouds have minimum values during winter season and maximum values in monsoon season (Figure 9a-c). Whereas DCC have minimum thickness in winter and maximum in pre-monsoon season (Figure 9d). The average cloud base (cloud top) altitudes for low-, middle-, high-level clouds and deep convective clouds are 1.74 km (3.16 km), 3.59 km (5.55 km), 8.79 km (10.49 km), and 1.22 km (11.45 km), respectively.Over Indian summer monsoon region,Das et al. (2017) reported that the percentage occurrence of high-level clouds is more than the other three cloud types. Over Shouxian (32.56^{o} N, 116.78^{o} E) location, Zhang et al. (2010) reported that the percentage

occurrence of low-, middle-, high-level clouds and deep convective cloudsis 20.1%, 19.3%, 59.5%, and 1.1%, respectively.

4.2.1. Single-layer and Multi-layer clouds

By interacting with both shortwave and longwave radiation, clouds play crucial role in the radiative budget at the surface, within and at the top of the atmosphere. Over the tropics, the zonal mean net cloud radiative effect differences between multi-layer clouds and single-layer clouds were positive and dominated by the shortwave cloud radiative effect differences (Li et al., 2011). This is because, the multi-layer clouds reflect less sunlight to the top of the atmosphere and transmit more to the surface and within the atmosphere than the single-layer clouds as a whole. As a result, multi-layer clouds warm the earth-atmosphere system when compared to single-layer clouds (Li et al., 2011). In this study, we studied the occurrence of single-layer and multi-layer clouds obtained during different seasons at Gadanki location. The percentage occurrence of single-layer, two-layer, three-layer and four- or more- layer clouds during pre-monsoon, monsoon, post-monsoon and winter seasons are shown in Figure 10(a-d). Single-layer, two-layer and three-layer clouds account for 40.80%, 30.71%, and 19.68% of all cloud configurations, respectively. Even though the low frequency of occurrence of one-layer clouds over Gadanki, they exhibit pronounced seasonal variation in magnitude with very low frequency during pre-monsoon season. This may be due to the strong warm and dry atmospheric conditions from surface to boundary layer top (Figure 4a and 4b). Percentage occurrence of single-layer (multi-layer) clouds during pre-monsoon, monsoon, post-monsoon and winter seasons are 7.7%, 14.2%, 8.48% and 10.42% (7.93%, 34.58%, 10.83% and 5.86%), respectively. There is a significant occurrence of multi-layer clouds during monsoon season than other seasons indicating that the development of multi-layer clouds is favorable under warm and moist atmospheric conditions (Figures 4a and 4b). Among the different cloud layers, the two-layer clouds have maximum percentage occurrence

(16.6%) during monsoon season (Figure 10b). Luo et al. (2009) reported the occurrence of multi-layer clouds over the Indian region during the summer season and attributed it to the complex cloud structure associated with the monsoon system. Zhang et al. (2010) reported that multi-layer cloud occurrence frequency is relatively higher during summer months (Jun., Jul. and Aug.) than autumn months (Sep., Oct. and Nov.) over Shouxian. Recently, Using the four years of combined observations of Cloudsat and CALIPSO, Subrahmanyam and Kumar (2017) reported the maximum frequency of occurrence of two-layer clouds over Indian sub-continent during Jun. Jul. and Aug months. This they attributed to the presence of Indian summer monsoon circulation over this region, which is dominated by the formation of various kinds of clouds such as cumulus, stratocumulus, cirrus etc.Very recently, George et al. (2018) reported CVS using the radiosonde launches during depression (D) and non-depression (ND) events in South West monsoon season using one month of field campaign data over Kanpur, India.

Figure 11(a-c) describe the mean vertical locations (base and top) and cloud thicknesses of single-layer, two-layer and three-layer clouds during different seasons. Except during winter season, single-layer clouds are thicker than the layers forming multi-layer clouds. Also, upper layer clouds are thicker than lower layer clouds in multi-layer clouds. This could be due to interactions between the different layers of cloud. This feature might also be associated with the strong reduction in longwave radiation cooling at the top of the lower layer of cloud in the presence of upper layers of cloud (Zhang et al., 2010; Wang et al., 1999; Chen and Cotton, 1987).

Irrespective of the season, single-layer clouds are high-level clouds i.e cloud base is > 5 km (Figure 11a). Maximum cloud top altitude and the cloud thickness occurred during monsoon season for single-layer clouds (Figure 11a) and the uppermost layer of multi-layer cloud configurations (Figure 11b-c). This is consistent with the low OLR values (< 220 W

475 m^{-2}) observed during monsoon season (Figure 11d). Except during pre-monsoon season,
476 cloud base, cloud top and cloud thickness values of lower layer of multi-layer clouds are
477 same during monsoon, post-monsoon and winter seasons. Whereas during pre-monsoon
478 season, cloud base and cloud top of lower layer of multi-layer clouds occurred at relatively
479 higher altitudes (Figure 11b-c). Similarly, there are no significant variations in cloud
480 thickness in middle layer of three-layer clouds between the seasons. However, cloud base and
481 cloud top of middle layer of three-layer clouds during pre-monsoon season occurred
482 relatively at higher altitudes than the other three seasons (Figure 11c). Table 2 describes the
483 mean base, top and thicknesses of cloud layers of single-layer, two-layer and three-layer
484 clouds. In the two-layer clouds, the thickness of the upper level cloud layer is about the same
485 as those of single-layer clouds. In the three-layer clouds, the base and top heights of the
486 lowest layer of cloud are similar to those of the lowest layer of cloud in two-layer clouds.

487 **4.3. Variability in CVS with respect to SW monsoon arrival over Gadanki**

488 CVS play an important role in the summer monsoon because they can significantly affect
489 the atmospheric heat balance through latent heating caused by water phase changes and
490 through scattering of radiation. In this section we discuss the variability in different clouds
491 with respect to the date of arrival of southwest (SW) monsoon over Gadanki. SW monsoon
492 onset occurs over Kerala coast (south west coast of India) during the last week of the May or
493 first week of June. In general, the climatological mean monsoon onset over Kerala (MOK) is
494 on 1 June with ± 7days. It is to be noted that the climatology onset date is obtained from IMD
495 long term onset dates and arrival date over Gadanki is picked up manually from the yearly
496 onset date lines over India map given by IMD.

497 Figure 12 shows the composite (2006 – 2016) percentage occurrence of clear sky and
498 cloud days (Figure 12a), low-level, middle-level, high-level and deep convective clouds
499 (Figure 12b), and one-, two-, three- and four or more- layer clouds (Figure 12c) with respect

to monsoon arrival date. Figures 13(a-c) describe the mean vertical locations (base and top) and cloud thicknesses of single-layer, two-layer clouds with respect to monsoon arrival date. Day zero in Figures 12(a-b) and Figures 13(a-b) indicates the date of monsoon arrival over Gadanki location. The percentages occurrence of clear sky conditions prior to the monsoon arrival over Gadanki location decreases and reduce to zero on the date of monsoon arrival (Figure 12a). This indicates the estimated dates of monsoon arrival over Gadanki location are correct. From day four onwards the cloudiness start increases and peaks on day 18 (Figure 12a). The percentage occurrence of middle level clouds decreases till 5 days prior to the monsoon arrival (Figure 12b). Subsequently middle level clouds percentage increases and does not show significant variability later to the monsoon arrival. There are no deep convective clouds prior and during the monsoon arrival over Gadanki location (Figure 12b). They occurred on day 3, 9, 10, 17 and 20. During and later to the arrival of the monsoon, the percentage occurrence of multilayer clouds is always greater than the single layer clouds except day three and four (Figure 12c). Day zero it is noted that single layer clouds are high level clouds and they are thicker with thickness ~ 6.7 km (Figure 13a). In two layer clouds the bottom layer is middle layer cloud and top layer is high level cloud (Figure 13b). The bottom layer is thicker than the top layer.During deep convective clouds and middle level, single layer clouds prevailed. The thickness of single layer clouds show large variability with thickness ranging from 300 m to 5 km during the first week later to the arrival of the monsoon. In the second week, the thickness ranges from 2 km to 5 km (Figure 13a). Later to the arrival of the monsoon, thickness of bottom layer in two layer cloud is relatively higher than the top layer (Figure 13b). Thicker single layer clouds and bottom layer of two layer clouds later to the monsoon arrival over Gadanki is due to the increase of tropospheric water vapor.

5. Summary

Cloud vertical structure (CVS) is studied for the first time over India by using long-term high vertical resolution radiosonde measurements at Gadanki location obtained during Apr. 2006 to May 2017. In order to obtain diurnal variation in CVS, we have used 3 hourly launched radiosondes for 72 hours in each month during Dec. 2010 to Mar. 2014. CVS is obtained following Zhang et al. (2010) where it relay on height-resolved relative humidity thresholds. After obtaining the cloud layers they are segregated to low, middle and high level clouds depending upon their altitude of occurrence. Detected layers are verified using independent measurements from cloud particle sensor (CPS) sonde launched from same location. Very good match between these two independent measurements is noticed.

First, the diurnal variations in CVS over Gadanki is studied using radiosonde observations taken from TTD campaigns conducted during CAWSES India Phase II program. During pre-monsoon and monsoon seasons, thickness of single-layer clouds reaches a maximum at 23 LT and a minimum at 14 LT. Upper layer of two–layer clouds show a maximum in thickness at 23 LT and minimum at 11 LT during monsoon season. Radiosonde measurements around 1730 LT were used to study the seasonal variability in CVS. After ascertaining the cloud layers they are segregated into different season to obtain the season variation of CVS. High-level clouds account for 69.05%, 58.49%, 55.5%, and 58.6% of cloud layers identified during pre-monsoon, monsoon, post-monsoon, and winter seasons, respectively, indicating high cloud layers being most prevalent at Gadanki location. Single-layer, two-layer, and three-layer clouds account for 40.80%, 30.71%, and 19.68% of all cloud configurations, respectively. Multi-layer clouds occurred more frequently during the monsoon with 34.58%. Maximum cloud top altitude and the cloud thickness occurred during monsoon season for single-layer clouds and the uppermost layer of multi-layer cloud configurations.

549 Further, we have discussed the variability in different clouds with respect to the date of
550 arrival of southwest (SW) monsoon over Gadanki location. Prior, during and later to the SW
551 monsoon arrival over Gadanki location, high level clouds occurrence is more than the other
552 cloud types. Whereas the middle level cloud occurrence decreases till 5 days prior to the
553 monsoon arrival and increases subsequently. There are no deep convective clouds prior and
554 during the monsoon arrival over Gadanki location.The thickness of single layer clouds shows
555 large variability during the first week later to the arrival of the monsoon. But it increases
556 significantly between 8 – 11 days later to the monsoon arrival. Later to the arrival of the
557 monsoon, thickness of bottom layer in two layer cloud is relatively higher than the top layer.
558 Thicker single layer clouds and bottom layer of two layer clouds later to the monsoon arrival
559 over Gadanki is due to the increase of tropospheric water vapor.

560 These cloud layers are expected to affect significantly to the background temperature
561 in the troposphere and lower stratosphere. The composite (2006-2016) temperature profiles
562 during clear sky, one-layer, two-layer, three-layer and four or more-layer cloud occurrences
563 are shown in Figure 14. The temperature differences between the cloudy (single-, two-, three-
564 , four or more- layer) and clear sky conditions are shown with dash lines in Figure 14. The
565 striking result here is that occurrence of peak cooling (peak warming) below (above) the Cold
566 Point Tropopause (CPT) altitude. The magnitude of cooling (warming) increases from single-
567 layer to four or more-layer cloud occurrence. The peak cooling and warming during four or
568 more-layer cloud occurrence are 0.9 K (at 15.7 km) and 3.6 K (at 18.1 K).Both single-layer
569 and multi-layer clouds show warming between 5 km and 14.5 km altitude region. The peak
570 warming of 0.8 K at 9.5 km for single-layer cloud, and 1.3 K at 10.2 K for multi-layer clouds
571 are observed and these altitudes are close to the cloud top altitude of single layer cloud and
572 top layer of multi-layer clouds (Table 2). The detailed study on the impact of single-layer and
573 multi-layer clouds on upper troposphere and lower stratosphere (UTLS) dynamics and

574 thermodynamics structure will be investigated in our subsequent article including their
575 radiative forcing.

576 **Acknowledgements**

577 We are grateful to the National Atmospheric Research Laboratory (NARL), Gadanki, for
578 providing necessary data for the present study.

579 **References**

580 Basha, G., Ratnam, M.V.: Moisture variability over Indian monsoon regions observed using
581 high resolution radiosonde measurements. Atmos. Res. 132–133, 35–45.
582 doi:10.1016/j.atmosres.2013.04.004, 2013.

583 Basha, G., Ratnam, M.V.: Identification of atmospheric boundary layer height over a tropical
584 station using high-resolution radiosonde refractivity profiles: Comparison with GPS radio
585 occultation measurements. J. Geophys. Res. Atmos. 114, D16101.
586 doi:10.1029/2008JD011692, 2009.

587 Behrangi, A., Kubar, T., Lambrigtsen, B.: Phenomenological Description of Tropical Clouds
588 Using CloudSat Cloud Classification. Mon. Weather Rev. 140, 3235–3249.
589 doi:10.1175/MWR-D-11-00247.1, 2012.

590 Biondi, R., Randel, W. J., Ho, S.-P., Neubert, T. and Syndergaard, S.: Thermal structure of
591 intense convective clouds derived from GPS radio occultations, Atmos. Chem. Phys., 12(12),
592 5309–5318, doi:10.5194/acp-12-5309-2012, 2012.

593 Biondi, R., Ho, S.-P., Randel, W.J., Neubert, T., Syndergaard, S.:Tropical cyclone cloud-top
594 height and vertical temperature structure detection using GPS radio occultation
595 measurements. J. Geophys. Res. Atmos. 118, 5247–5259. doi:10.1002/jgrd.50448, 2013.

596 Biondi, R., Steiner, A. K., Kirchengast, G., Brenot, H. and Rieckh, T.: Supporting the
597 detection and monitoring of volcanic clouds: A promising new application of Global

598 Navigation Satellite System radio occultation, Adv. Sp. Res., 60(12), 2707–2722, doi:
599 10.1016/j.asr.2017.06.039, 2017.
600 Blaskovic, M., Davies, R., Snider, J.B.: Diurnal Variation of Marine Stratocumulus over San
601 Nicolas Island during July 1987. Mon. Weather Rev. 119, 1469–1478. doi:10.1175/1520-
602 0493(1991)119<1469:DVOMSO>2.0.CO;2, 1990.
603 Cesana, G., Chepfer, H.: How well do climate models simulate cloud vertical structure? A
604 comparison between CALIPSO-GOCCP satellite observations and CMIP5 models. Geophys.
605 Res. Lett. 39, n/a-n/a. doi:10.1029/2012GL053153, 2012.
606 Chahine, M.T., Pagano, T.S., Aumann, H.H., Atlas, R., Barnet, C., Blaisdell, J., Chen, L.,
607 Divakarla, M., Fetzer, E.J., Goldberg, M., Gautier, C., Granger, S., Hannon, S., Irion, F.W.,
608 Kakar, R., Kalnay, E., Lambrigtsen, B.H., Lee, S.-Y., Le Marshall, J., McMillan, W.W.,
609 McMillin, L., Olsen, E.T., Revercomb, H., Rosenkranz, P., Smith, W.L., Staelin, D., Strow,
610 L.L., Susskind, J., Tobin, D., Wolf, W., Zhou, L.: AIRS: Improving Weather Forecasting and
611 Providing New Data on Greenhouse Gases. Bull. Am. Meteorol. Soc. 87, 911–926.
612 doi:10.1175/BAMS-87-7-911, 2006.
613 Chen, C., Cotton, W.R.: The Physics of the Marine Stratocumulus-Capped Mixed Layer. J.
614 Atmos. Sci. 44, 2951–2977. doi:10.1175/1520-0469(1987)044<2951:TPOTMS>2.0.CO;2,
615 1987.
616 Chernykh, I. V, Eskridge, R.E.: Determination of Cloud Amount and Level from Radiosonde
617 Soundings. J. Appl. Meteorol. 35, 1362–1369. doi:10.1175/1520-
618 0450(1996)035<1362:DOCAAL>2.0.CO;2, 1996.
619 Costa-Surós, M., Calbó, J., González, J.A., Long, C.N.:: Comparing the cloud vertical
620 structure derived from several methods based on radiosonde profiles and ground-based
621 remote sensing measurements. Atmos. Meas. Tech. 7, 2757–2773. doi:10.5194/amt-7-2757-
622 2014, 2014.

623 Crewell, S., Bloemink, H., Feijt, A., García, S.G., Jolivet, D., Krasnov, O.A., Van Lammeren,
624 A., Löhnert, U., Van Meijgaard, E., Meywerk, J., Quante, M., Pfeilsticker, K., Schmidt, S.,
625 Scholl, T., Simmer, C., Schröder, M., Trautmann, T., Venema, V., Wendisch, M., Willén, U.:
626 THE BALTEX BRIDGE CAMPAIGN: An Integrated Approach for a Better Understanding
627 of Clouds. Bull. Am. Meteorol. Soc. 85, 1565–1584. doi:10.1175/BAMS-85-10-1565, 2004.
628 Das, S.K., Golhait, R.B., Uma, K.N.: Clouds vertical properties over the Northern
629 Hemisphere monsoon regions from CloudSat-CALIPSO measurements. Atmos. Res. 183,
630 73–83. doi:https://doi.org/10.1016/j.atmosres.2016.08.011, 2017.
631 de Beek, R., Vountas, M., Rozanov, V. V., Richter, a., and Burrows, J. P.: The ring effect in
632 the cloudy atmosphere, Geophys. Res. Lett., 28, 721–724, doi:10.1029/2000GL012240,
633 2001.
634 Eresmaa, N., Karppinen, A., Joffre, S.M., Räsänen, J., Talvitie, H.: Mixing height
635 determination by ceilometer. Atmos. Chem. Phys. 6, 1485–1493. doi:10.5194/acp-6-1485-
636 2006, 2006.
637 Fujiwara, M., Sugidachi, T., Arai, T., Shimizu, K., Hayashi, M., Noma, Y., Kawagita, H.,
638 Sagara, K., Nakagawa, T., Okumura, S., Inai, Y., Shibata, T., Iwasaki, S., Shimizu, A.;
639 Development of a cloud particle sensor for radiosonde sounding. Atmos. Meas. Tech. 9,
640 5911–5931. doi:10.5194/amt-9-5911-2016, 2016.
641 Gambheer, A. V, Bhat, G.S.: Diurnal variation of deep cloud systems over the Indian region
642 using INSAT-1B pixel data. Meteorol. Atmos. Phys. 78, 215–225. doi:10.1007/s703-001-
643 8175-4, 2001.
644 George, G., Sarangi, C., Tripathi, S. N., Chakraborty, T., & Turner, A.: Vertical structure and
645 radiative forcing of monsoon clouds over Kanpur during the 2016 INCOMPASS field
646 campaign. J. Geophys. Res., 123. https://doi.org/10.1002/2017JD027759, 2018.

647 Goloub, P., Deuze, J. L., Herman, M., and Fouquart, Y.: Analysis of the POLDER
648 polarization measurements performed over cloud covers, IEEE T. Geosci. Remote, 32, 78–
649 88, doi:10.1109/36.285191, 1994.
650 Hahn, C.J., Rossow, W.B., Warren, S.G.: ISCCP Cloud Properties Associated with Standard
651 Cloud Types Identified in Individual Surface Observations. J. Clim. 14, 11–28.
652 doi:10.1175/1520-0442(2001)014<0011:ICPAWS>2.0.CO;2, 2001.
653 Heintzenberg, J., Charlson, R.J. (Eds.): Clouds in the perturbed climate system: their
654 relationship to energy balance, atmospheric dynamics and precipitation. MIT Press,
655 Cambridge, UK, 2009.
656 Huang, Y.: On the Longwave Climate Feedbacks. J. Clim. 26, 7603–7610. doi:10.1175/JCLI-
657 D-13-00025.1, 2013.
658 Jiang, X., Waliser, D.E., Li, J.-L., Woods, C.: Vertical cloud structures of the boreal summer
659 intraseasonal variability based on CloudSat observations and ERA-interim reanalysis. Clim.
660 Dyn. 36, 2219–2232. doi:10.1007/s00382-010-0853-8, 2011.
661 Joiner, J. and Bhartia, P. K.: The determination of cloud pressures from rotational Raman
662 scattering in satellite backscatter ultraviolet measurements, J. Geophys. Res., 100, 23019–
663 23026, doi:10.1029/95JD02675, 1995.
664 Kim, S.-W., Chung, E.-S., Yoon, S.-C., Sohn, B.-J., Sugimoto, N.: Intercomparisons of
665 cloud-top and cloud-base heights from ground-based Lidar, CloudSat and CALIPSO
666 measurements. Int. J. Remote Sens. 32, 1179–1197. doi:10.1080/01431160903527439, 2011.
667 Lazarus, S.M., Krueger, S.K., Mace, G.G.: A Cloud Climatology of the Southern Great Plains
668 ARM CART. J. Clim. 13, 1762–1775. doi:10.1175/1520-
669 0442(2000)013<1762:ACCOTS>2.0.CO;2, 2000.
670 King, N. J. and Vaughan, G.: Using passive remote sensing to retrieve the vertical variation
671 of cloud droplet size in marine stratocumulus: An assessment of information content and the

potential for improved retrievals from hyperspectral measurements, J. Geophys. Res., 117, D15206, doi:10.1029/2012JD017896, 2012.

Knibbe, W. J. J., De Haan, J. F., Hovenier, J. W., Stam, D. M., Koelemeijer, R. B. A., and Stammes, P.: Deriving terrestrial cloud top pressure from photopolarimetry of reflected light, J. Quant. Spectrosc. Ra., 64, 173–199, doi:10.1016/S0022-4073(98)00135-6, 2000.

L'Ecuyer, T. ~S., Jiang, J. ~H.: Touring the atmosphere aboard the A-Train. Phys. Today 63, 36. doi:10.1063/1.3463626, 2010.

Li, J., Yi, Y., Minnis, P., Huang, J., Yan, H., Ma, Y., Wang, W., Kirk Ayers, J.: Radiative effect differences between multi-layered and single-layer clouds derived from CERES, CALIPSO, and CloudSat data. J. Quant. Spectrosc. Radiat. Transf. 112, 361–375. doi:https://doi.org/10.1016/j.jqsrt.2010.10.006, 2011.

Li, Y., Liu, X., Chen, B.: Cloud type climatology over the Tibetan Plateau: A comparison of ISCCP and MODIS/TERRA measurements with surface observations. Geophys. Res. Lett. 33, n/a-n/a. doi:10.1029/2006GL026890, 2006.

Li, Z., Barker, H.W., Moreau, L.: The variable effect of clouds on atmospheric absorption of solar radiation. Nature 376, 486–490, 1995.

Li, Z., Cribb, M.C., Chang, F.-L., Trishchenko, A., Luo, Y.: Natural variability and sampling errors in solar radiation measurements for model validation over the Atmospheric Radiation Measurement Southern Great Plains region. J. Geophys. Res. Atmos. 110, n/a-n/a. doi:10.1029/2004JD005028, 2005.

Luo, Y., Zhang, R., Wang, H.: Comparing Occurrences and Vertical Structures of Hydrometeors between Eastern China and the Indian Monsoon Region Using CloudSat/CALIPSO Data. J. Clim. 22, 1052–1064. doi:10.1175/2008JCLI2606.1, 2009.

Merlin, G., Riedi, J., Labonnote, L. C., Cornet, C., Davis, A. B., Dubuisson, P., Desmons, M., Ferlay, N., and Parol, F.: Cloud information content analysis of multi-angular

measurements in the oxygen A-band: application to 3MI and MSPI, Atmos. Meas. Tech., 9, 4977-4995, doi:amt-9-4977-2016, 2016.

Minnis, P., Yi, Y., Huang, J., Ayers, K.: Relationships between radiosonde and RUC-2 meteorological conditions and cloud occurrence determined from ARM data. J. Geophys. Res. Atmos. 110, n/a-n/a. doi:10.1029/2005JD006005, 2005.

Moroney, C., Davies, R., and Muller, J.-P.: Operational retrieval of cloud-top heights using MISR data, IEEE T. Geosci. Remote, 40, 1532–1540, doi:10.1109/TGRS.2002.801150, 2002.

Nath, D., Venkat Ratnam, M., Jagannadha Rao, V.V.M., Krishna Murthy, B. V, Vijaya Bhaskara Rao, S.: Gravity wave characteristics observed over a tropical station using high-resolution GPS radiosonde soundings. J. Geophys. Res. Atmos. 114, n/a-n/a. doi:10.1029/2008JD011056, 2009.

Naud, C.M., Chen, Y.-H.: Assessment of ISCCP cloudiness over the Tibetan Plateau using CloudSat-CALIPSO. J. Geophys. Res. Atmos. 115, n/a-n/a. doi:10.1029/2009JD013053, 2010.

Naud, C.M., Muller, J.-P., Clothiaux, E.E.: Comparison between active sensor and radiosonde cloud boundaries over the ARM Southern Great Plains site. J. Geophys. Res. Atmos. 108, n/a-n/a. doi:10.1029/2002JD002887, 2003.

Noh, Y.-J., Seaman, C.J., Vonder Haar, T.H., Hudak, D.R., Rodriguez, P.: Comparisons and analyses of aircraft and satellite observations for wintertime mixed-phase clouds. J. Geophys. Res. Atmos. 116, n/a-n/a. doi:10.1029/2010JD015420, 2011.

Nowak, D., Ruffieux, D., Agnew, J.L., Vuilleumier, L.: Detection of Fog and Low Cloud Boundaries with Ground-Based Remote Sensing Systems. J. Atmos. Ocean. Technol. 25, 1357–1368. doi:10.1175/2007JTECHA950.1, 2008.

Pallamraju, D., Gurubaran, S., Venkat Ratnam, M.: A brief overview on the special issue on

722 CAWSES-India Phase II program. J. Atmos. Solar-Terrestrial Phys. 121, 141–144.
723 doi:https://doi.org/10.1016/j.jastp.2014.10.013, 2014.
724 Platnick, S., King, M. D., Ackerman, S., Menzel, W. P., Baum, B., Riedi, J. C., and Frey, R.:
725 The MODIS cloud products: Algorithms and examples from Terra, IEEE T. Geosci. Remote,
726 41, 459–473, doi:10.1109/TGRS.2002.808301, 2003.
727 Poore, K.D., Wang, J., Rossow, W.B.: Cloud Layer Thicknesses from a Combination of
728 Surface and Upper-Air Observations. J. Clim. 8, 550–568. doi:10.1175/1520-
729 0442(1995)008<0550:CLTFAC>2.0.CO;2, 1995.
730 Qian, Y., Long, C.N., Wang, H., Comstock, J.M., McFarlane, S.A., Xie, S.: Evaluation of
731 cloud fraction and its radiative effect simulated by IPCC AR4 global models against ARM
732 surface observations. Atmos. Chem. Phys. 12, 1785–1810. doi:10.5194/acp-12-1785-2012,
733 2012.
734 Ramanathan, V., Cess, R.D., Harrison, E.F., Minnis, P., Barkstorm, B.R., Ahmad, E.,
735 Hartmann, D.: Cloud-Radiative Forcing and Climate: Results from the Earth Radiation
736 Budget Experiment. Science (80-.). 243, 57 LP-63,, 1989.
737 Randall, D.A.: Cloud parameterization for climate modeling: Status and prospects. Atmos.
738 Res. 23, 345–361. doi:https://doi.org/10.1016/0169-8095(89)90025-2, 1989.
739 Rao, T.N., Kirankumar, N.V.P., Radhakrishna, B., Rao, D.N., Nakamura, K.: Classification
740 of Tropical Precipitating Systems Using Wind Profiler Spectral Moments. Part II: Statistical
741 Characteristics of Rainfall Systems and Sensitivity Analysis. J. Atmos. Ocean. Technol. 25,
742 898–908. doi:10.1175/2007JTECHA1032.1, 2008a.
743 Ravi Kiran, V., Rajeevan, M., Gadhavi, H., Rao, S.V.B., Jayaraman, A.: Role of vertical
744 structure of cloud microphysical properties on cloud radiative forcing over the Asian
745 monsoon region. Clim. Dyn. 45, 3331–3345. doi:10.1007/s00382-015-2542-0, 2015.
746 Reddy, N.N., Rao, K.G.: Contrasting variations in the surface layer structure between the

747 convective and non-convective periods in the summer monsoon season for Bangalore
748 location during PRWONAM. J. Atmos. Solar-Terrestrial Phys. 167, 156-168.
749 doi:10.1016/j.jastp.2017.11.017, 2017, 2018.
750 Rind, D., Rossow, W.B.: The Effects of Physical Processes on the Hadley Circulation. J.
751 Atmos. Sci. 41, 479–507. doi:10.1175/1520-0469(1984)041<0479:TEOPPO>2.0.CO;2,
752 1984.
753 Roja Raman, M., Jagannadha Rao, V.V.M., Venkat Ratnam, M., Rajeevan, M., Rao, S.V.B.,
754 Narayana Rao, D., Prabhakara Rao, N.: Characteristics of the Tropical Easterly Jet: Long-
755 term trends and their features during active and break monsoon phases. J. Geophys. Res.
756 Atmos. 114, n/a-n/a. doi:10.1029/2009JD012065, 2009.
757 Rossow, W. B. and Schiffer, R. A.: ISCCP Cloud Data Products, B. Am. Meteorol. Soc., 72,
758 2–20, doi:10.1175/1520-0477(1991)072<0002:ICDP>2.0.CO;2, 1991.
759 Rossow, W.B., Garder, L.C.: Validation of ISCCP Cloud Detections. J. Clim. 6, 2370–2393.
760 doi:10.1175/1520-0442(1993)006<2370:VOICD>2.0.CO;2, 1993.
761 Rossow, W.B., Lacis, A.A.: Global, Seasonal Cloud Variations from Satellite Radiance
762 Measurements. Part II. Cloud Properties and Radiative Effects. J. Clim. 3, 1204–1253.
763 doi:10.1175/1520-0442(1990)003<1204:GSCVFS>2.0.CO;2, 1990.
764 Rossow, W.B., Zhang, Y.: Evaluation of a Statistical Model of Cloud Vertical Structure
765 Using Combined CloudSat and CALIPSO Cloud Layer Profiles. J. Clim. 23, 6641–6653.
766 doi:10.1175/2010JCLI3734.1, 2010.
767 Rossow, W.B., Zhang, Y., Wang, J.: A Statistical Model of Cloud Vertical Structure Based
768 on Reconciling Cloud Layer Amounts Inferred from Satellites and Radiosonde Humidity
769 Profiles. J. Clim. 18, 3587–3605. doi:10.1175/JCLI3479.1, 2005.
770 Sassen, K., Wang, Z.: Classifying clouds around the globe with the CloudSat radar: 1-year of
771 results. Geophys. Res. Lett. 35, n/a-n/a. doi:10.1029/2007GL032591, 2008.

772 Seiz, G., Tjemkes, S., and Watts, P.: Multiview Cloud-Top Height and Wind Retrieval with
773 Photogrammetric Methods: Application to Meteosat-8 HRV Observations, J. Appl. Meteorol.
774 Clim., 46,1182–1195, doi:10.1175/JAM2532.1, 2007.
775 Slingo, A., Slingo, J.M.: The response of a general circulation model to cloud longwave
776 radiative forcing. I: Introduction and initial experiments. Q. J. R. Meteorol. Soc. 114, 1027–
777 1062. doi:10.1002/qj.49711448209, 1988.
778 Slingo, J.M., Slingo, A.: The response of a general circulation model to cloud longwave
779 radiative forcing. II: Further studies. Q. J. R. Meteorol. Soc. 117, 333–364.
780 doi:10.1002/qj.49711749805, 1991.
781 Stephens, G.L.: Cloud Feedbacks in the Climate System: A Critical Review. J. Clim. 18,
782 237–273. doi:10.1175/JCLI-3243.1, 2005.
783 Stephens, G.L., Vane, D.G., Tanelli, S., Im, E., Durden, S., Rokey, M., Reinke, D., Partain,
784 P., Mace, G.G., Austin, R., L'Ecuyer, T., Haynes, J., Lebsock, M., Suzuki, K., Waliser, D.,
785 Wu, D., Kay, J., Gettelman, A., Wang, Z., Marchand, R.: CloudSat mission: Performance and
786 early science after the first year of operation. J. Geophys. Res. Atmos. 113, n/a-n/a.
787 doi:10.1029/2008JD009982, 2008.
788 Subrahmanyam, K.V., Kumar, K.K.: CloudSat observations of multi layered clouds across
789 the globe. Clim. Dyn. 49, 327–341. doi:10.1007/s00382-016-3345-7, 2017.
790 Uma, K.N., Kumar, K.K., Shankar Das, S., Rao, T.N., Satyanarayana, T.M.: On the Vertical
791 Distribution of Mean Vertical Velocities in the Convective Regions during the Wet and Dry
792 Spells of the Monsoon over Gadanki. Mon. Weather Rev. 140, 398–410. doi:10.1175/MWR-
793 D-11-00044.1, 2012.
794 Venkat Ratnam, M., Narendra Babu, A., Jagannadha Rao, V.V.M., Vijaya Bhaskar Rao, S.,
795 Narayana Rao, D.: MST radar and radiosonde observations of inertia-gravity wave
796 climatology over tropical stations: Source mechanisms. J. Geophys. Res. Atmos. 113, n/a-n/a.

797 doi:10.1029/2007JD008986, 2008.

798 Venkat Ratnam, M., Pravallika, N., Ravindra Babu, S., Basha, G., Pramitha, M., Krishna
799 Murthy, B. V.: Assessment of GPS radiosonde descent data. Atmos. Meas. Tech. 7, 1011–
800 1025. doi:10.5194/amt-7-1011-2014, 2014a.

801 Venkat Ratnam, M., Sunilkumar, S. V, Parameswaran, K., Krishna Murthy, B. V,
802 Ramkumar, G., Rajeev, K., Basha, G., Ravindra Babu, S., Muhsin, M., Kumar Mishra, M.,
803 Hemanth Kumar, A., Akhil Raj, S.T., Pramitha, M.: Tropical tropopause dynamics (TTD)
804 campaigns over Indian region: An overview. J. Atmos. Solar-Terrestrial Phys. 121, 229–239.
805 doi:https://doi.org/10.1016/j.jastp.2014.05.007, 2014b.

806 Wang, F., Xin, X., Wang, Z., Cheng, Y., Zhang, J., Yang, S.: Evaluation of cloud vertical
807 structure simulated by recent BCC_AGCM versions through comparison with CALIPSO-
808 GOCCP data. Adv. Atmos. Sci. 31, 721–733. doi:10.1007/s00376-013-3099-7, 2014.

809 Wang, J., Rossow, W.B.: Effects of Cloud Vertical Structure on Atmospheric Circulation in
810 the GISS GCM. J. Clim. 11, 3010–3029. doi:10.1175/1520-
811 0442(1998)011<3010:EOCVSO>2.0.CO;2, 1998.

812 Wang, J., Rossow, W.B.: Determination of Cloud Vertical Structure from Upper-Air
813 Observations. J. Appl. Meteorol. 34, 2243–2258. doi:10.1175/1520-
814 0450(1995)034<2243:DOCVSF>2.0.CO;2, 1995.

815 Wang, J., Rossow, W.B., Uttal, T., Rozendaal, M.: Variability of Cloud Vertical Structure
816 during ASTEX Observed from a Combination of Rawinsonde, Radar, Ceilometer, and
817 Satellite. Mon. Weather Rev. 127, 2484–2502. doi:10.1175/1520-
818 0493(1999)127<2484:VOCVSD>2.0.CO;2, 1999.

819 Wang, J., Rossow, W.B., Zhang, Y.: Cloud Vertical Structure and Its Variations from a 20-Yr
820 Global Rawinsonde Dataset. J. Clim. 13, 3041–3056. doi:10.1175/1520-
821 0442(2000)013<3041:CVSAIV>2.0.CO;2, 2000.

822 Warren, S.G., Hahn, C.J., London, J., Chervin, R.M., Jenne, R.L.: Global distribution of total
823 cloud cover and cloud type amounts over the ocean. doi:TN-317+STR, 212 pp, 1988.
824 Wielicki, B.A., Harrison, E.F., Cess, R.D., King, M.D., Randall, D.A. Mission to Planet
825 Earth: Role of Clouds and Radiation in Climate. Bull. Am. Meteorol. Soc. 76, 2125–2153.
826 doi:10.1175/1520-0477(1995)076<2125:MTPERO>2.0.CO;2, 1995.
827 Winker, D.M., Hunt, W.H., McGill, M.J.; Initial performance assessment of CALIOP.
828 Geophys. Res. Lett. 34, n/a-n/a. doi:10.1029/2007GL030135, 2007.
829 Wu, D. L., Ackerman, S. a., Davies, R., Diner, D. J., Garay, M. J., Kahn, B. H., Maddux, B.
830 C., Moroney, C. M., Stephens, G. L., Veefkind, J. P., and Vaughan, M. A.: Vertical
831 distributions and relationships of cloud occurrence frequency as observed by MISR, AIRS,
832 MODIS, OMI, CALIPSO, and CloudSat, Geophys. Res. Lett., 36, L09821,
833 doi:10.1029/2009GL037464, 2009.
834 Xi, B., Dong, X., Minnis, P., Khaiyer, M.M.: A 10 year climatology of cloud fraction and
835 vertical distribution derived from both surface and GOES observations over the DOE ARM
836 SPG site. J. Geophys. Res. Atmos. 115, n/a-n/a. doi:10.1029/2009JD012800, 2010.
837 Yang, Q., Fu, Q., Hu, Y.: Radiative impacts of clouds in the tropical tropopause layer. J.
838 Geophys. Res. Atmos. 115, n/a-n/a. doi:10.1029/2009JD012393, 2010.
839 Zhang, J., Chen, H., Li, Z., Fan, X., Peng, L., Yu, Y., Cribb, M.: Analysis of cloud layer
840 structure in Shouxian, China using RS92 radiosonde aided by 95 GHz cloud radar. J.
841 Geophys. Res. Atmos. 115, n/a-n/a. doi:10.1029/2010JD014030, 2010.
842 Zuidema, P.: Convective Clouds over the Bay of Bengal. Mon. Weather Rev. 131, 780–798.
843 doi:10.1175/1520-0493(2003)131<0780:CCOTBO>2.0.CO;2, 2003.
844

845 **Tables:**

846

	Height-resolving RH thresholds		
Altitude range	min-RH	max-RH	inter-RH
0-2 km	92%	95%	84%
2-6 km	90%	93%	82%
6-12 km	88%	90%	78%
>12 km	75%	80%	70%

847

848 **Table 1.** Summary of height-resolving RH thresholds.

849

	Multi-layer clouds	Cloud base altitude (km)	Cloud top altitude (km)	Cloud thickness (km)
	Single-layer cloud	6.32	9.24	2.92
Upper layer	two-layer clouds	8.51	11.23	2.72
	three-layer clouds	9.63	11.79	2.16
Middle layer	three-layer clouds	6.69	7.80	1.11
Lower layer	two-layer clouds	4.08	5.56	1.48
	three-layer clouds	3.04	4.31	1.27

850

851 **Table 2.** Mean base, top and thicknesses of cloud layers of single-layer, two-layer and three-
852 layer clouds.
853

854

855

856 **Figures:**

857

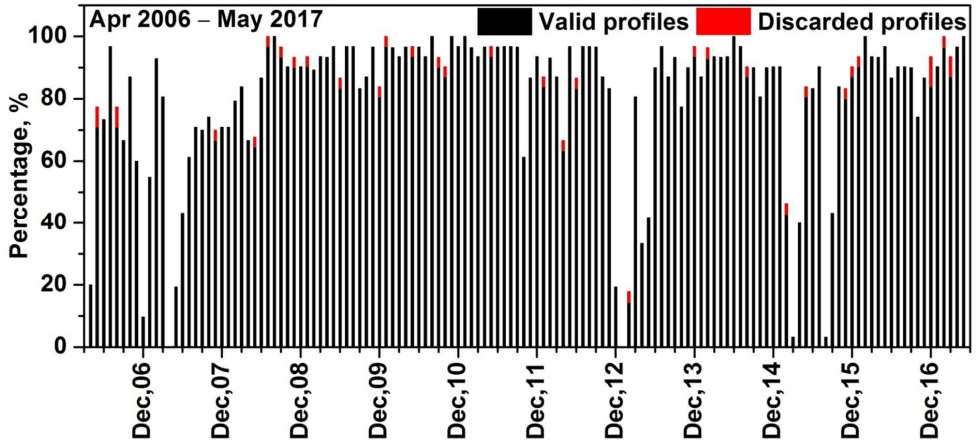

858

859 **Figure 1.** Monthly percentage of radiosonde data available during Apr. 2006 – May. 2017 at

860 Gadanki. Percentage of discarded profiles in each month is also shown with red colour.

861

Atmos. Chem. Phys. Discuss., https://doi.org/10.5194/acp-2018-194
Manuscript under review for journal Atmos. Chem. Phys.
Discussion started: 5 April 2018

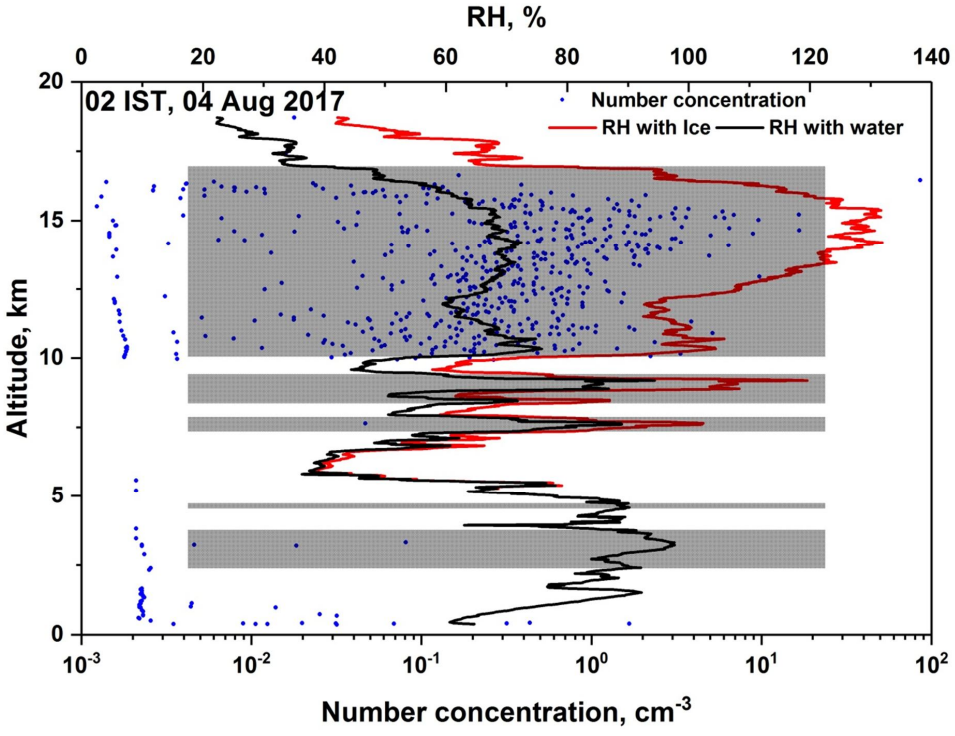

Figure 2. Results from a flight of RS-11G radiosonde and Cloud Particle Sensor (CPS) sonde on the same balloon launched at 02 IST on 04 Aug 2017 at Gadanki, India. Profiles of RH estimated with respect to water (black solid line) and ice (when temperatures are less than 0^{o}C (red solid line)), and number concentration (filled blue circles) from CPS sonde profile are shown. Detected cloud layer boundaries are shown by the filled gray rectangle boxes. Increase in the number concentration within the detected cloud layers indicates the cloud layer boundaries detected in the present study are accurate.

Atmos. Chem. Phys. Discuss., https://doi.org/10.5194/acp-2018-194
Manuscript under review for journal Atmos. Chem. Phys.
Discussion started: 5 April 2018

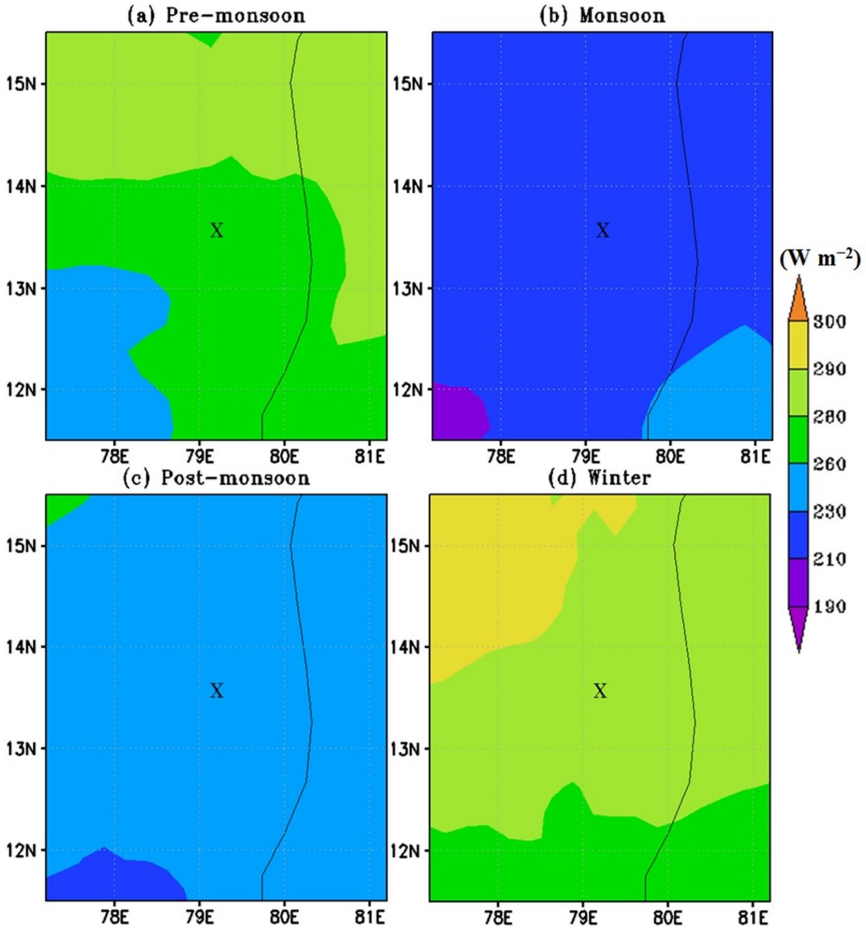

873

874 **Figure 3.** Seasonal mean distribution of OLR around Gadanki location observed during (a)
875 Pre-monsoon, (b) Monsoon, (c) Post-monsoon and (d) Winter seasons averaged during
876 2006 − 2017. The symbol 'X' indicates the location of Gadanki.

877

Atmos. Chem. Phys. Discuss., https://doi.org/10.5194/acp-2018-194
Manuscript under review for journal Atmos. Chem. Phys.
Discussion started: 5 April 2018

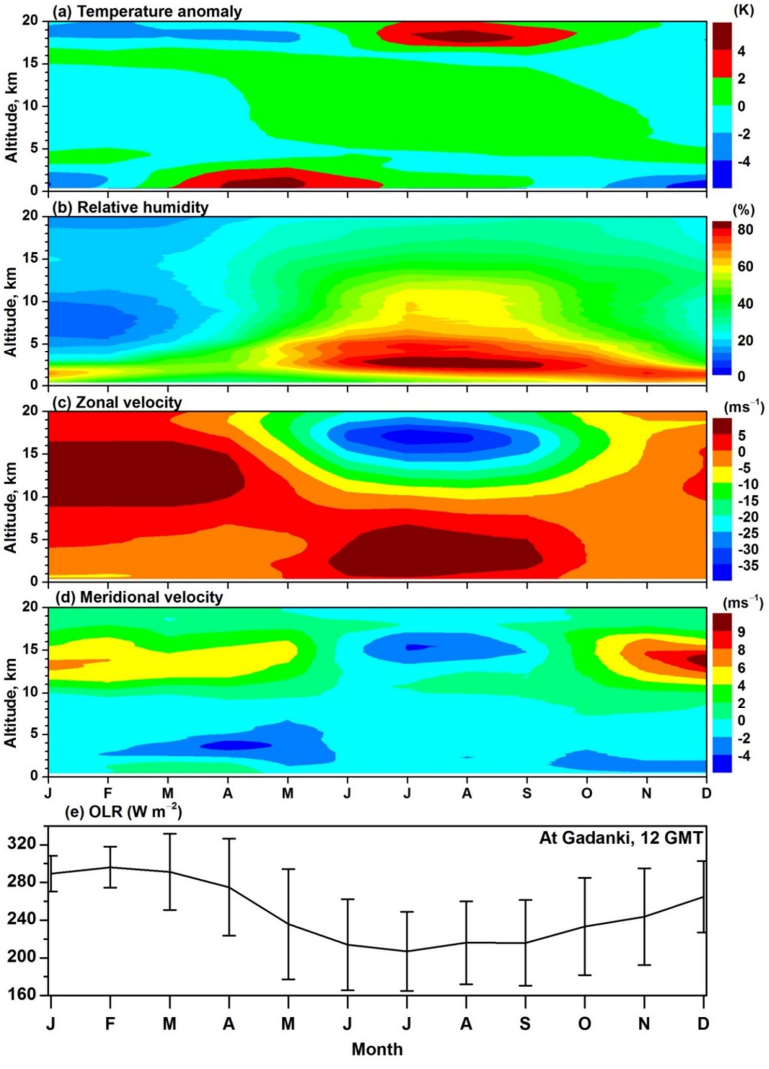

878

879 **Figure 4.** Time–altitude cross sections of monthly mean (a) Temperature anomaly, (b)
880 Relative humidity, (c) Zonal wind and (d) Meridional wind observed over Gadanki using
881 radiosonde observations during Apr. 2006 to May 2017. (e) Monthly mean Outgoing
882 Longwave Radiation (OLR) over Gadanki obtained using KALPANA-1 data during Apr.
883 2006 to May 2017 along with standard deviation (vertical bars).

884

Atmos. Chem. Phys. Discuss., https://doi.org/10.5194/acp-2018-194
Manuscript under review for journal Atmos. Chem. Phys.
Discussion started: 5 April 2018

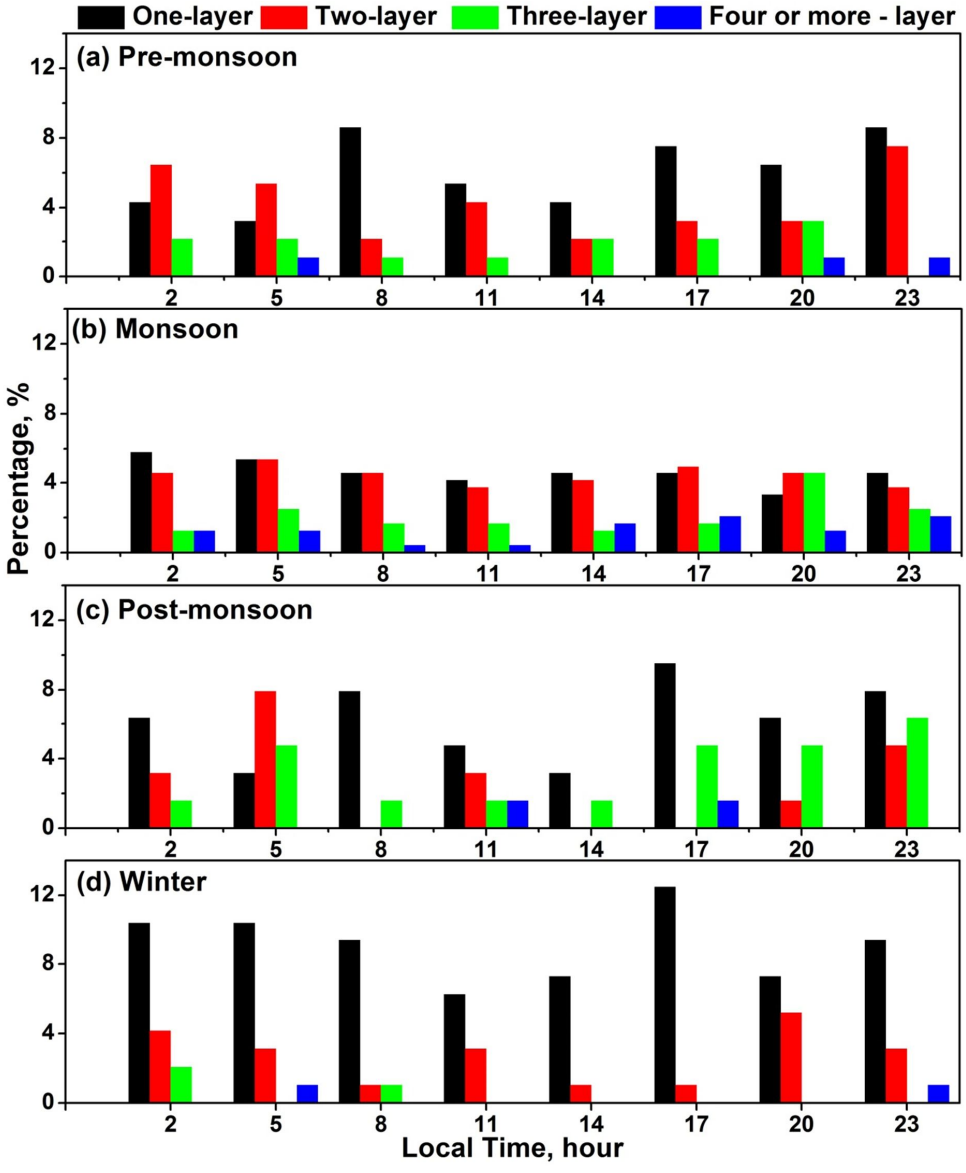

Figure 5. Diurnal variations of one-layer, two-layer, three-layer, and four- or more- layer clouds observed during (a) pre-monsoon, (b) monsoon, (c) post-monsoon, and (d) winter seasons.

Atmos. Chem. Phys. Discuss., https://doi.org/10.5194/acp-2018-194
Manuscript under review for journal Atmos. Chem. Phys.
Discussion started: 5 April 2018

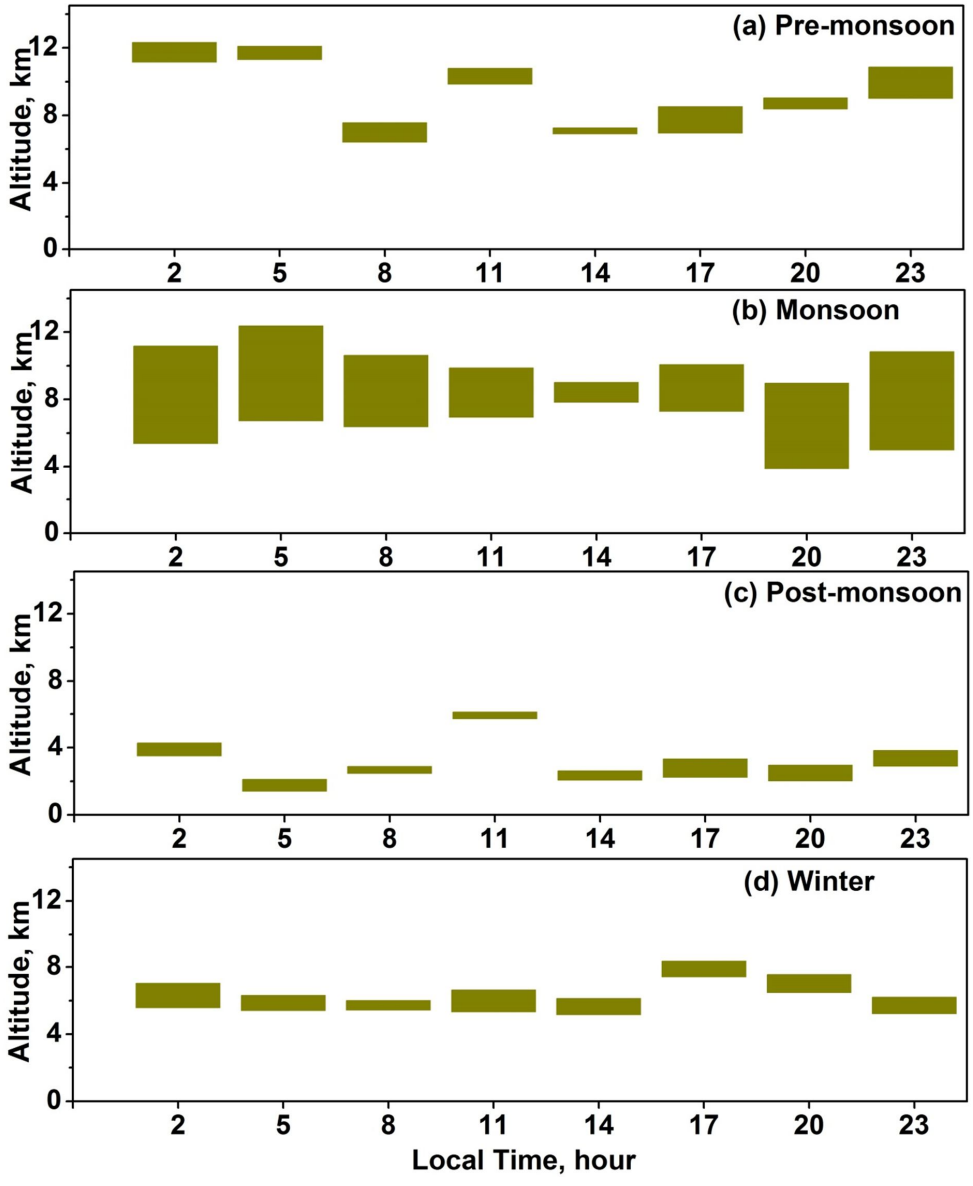

Figure 6. Diurnal variations of mean vertical locations (base and top), thicknesses of one-layer clouds observed during (a) pre-monsoon, (b) monsoon, (c) post-monsoon, and (d) winter seasons.

Atmos. Chem. Phys. Discuss., https://doi.org/10.5194/acp-2018-194
Manuscript under review for journal Atmos. Chem. Phys.
Discussion started: 5 April 2018

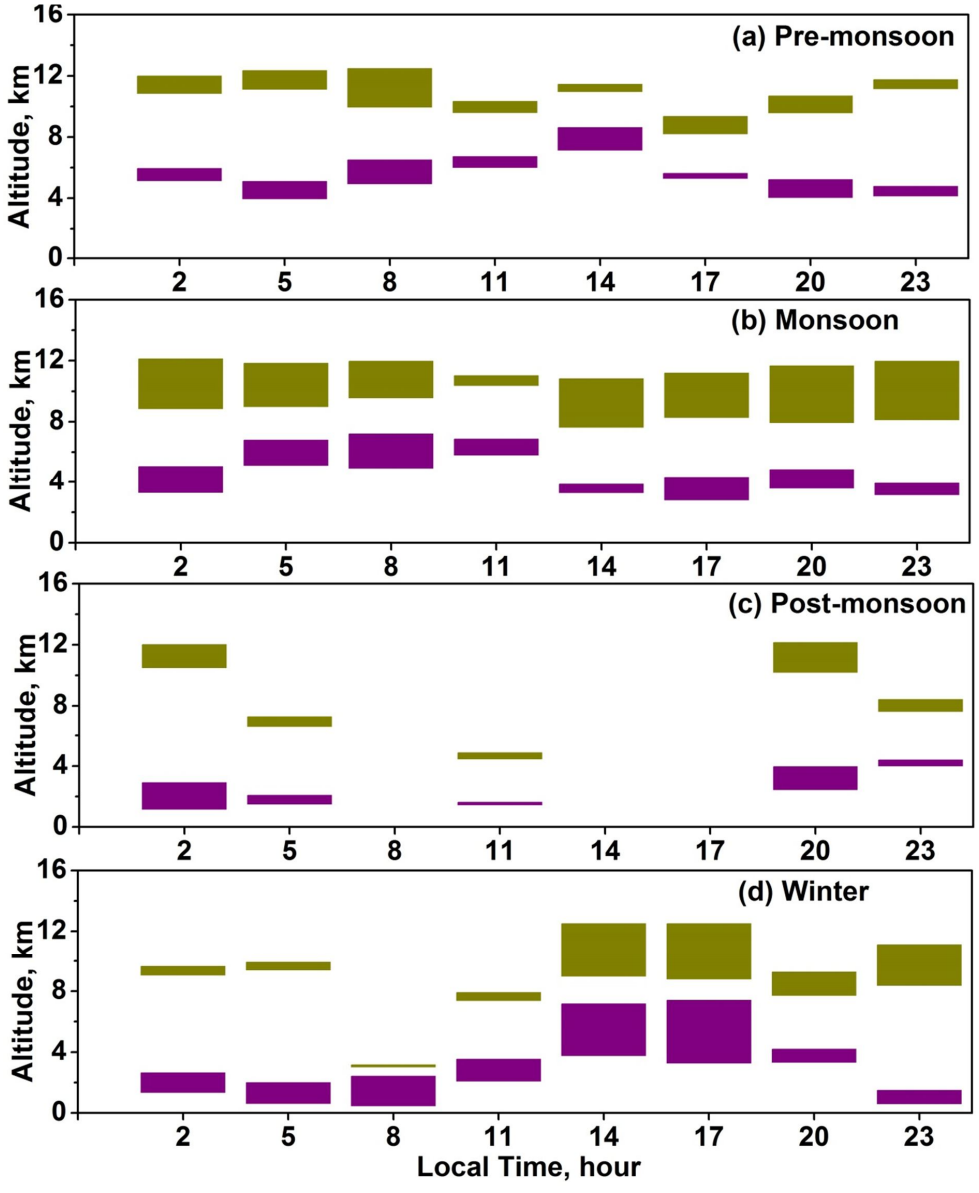

Figure 7. Diurnal variations of mean vertical locations (base and top), thicknesses of two-layer clouds observed during (a) pre-monsoon, (b) monsoon, (c) post-monsoon, and (d) winter seasons.

Atmos. Chem. Phys. Discuss., https://doi.org/10.5194/acp-2018-194
Manuscript under review for journal Atmos. Chem. Phys.
Discussion started: 5 April 2018

Atmospheric Chemistry and Physics Discussions

901

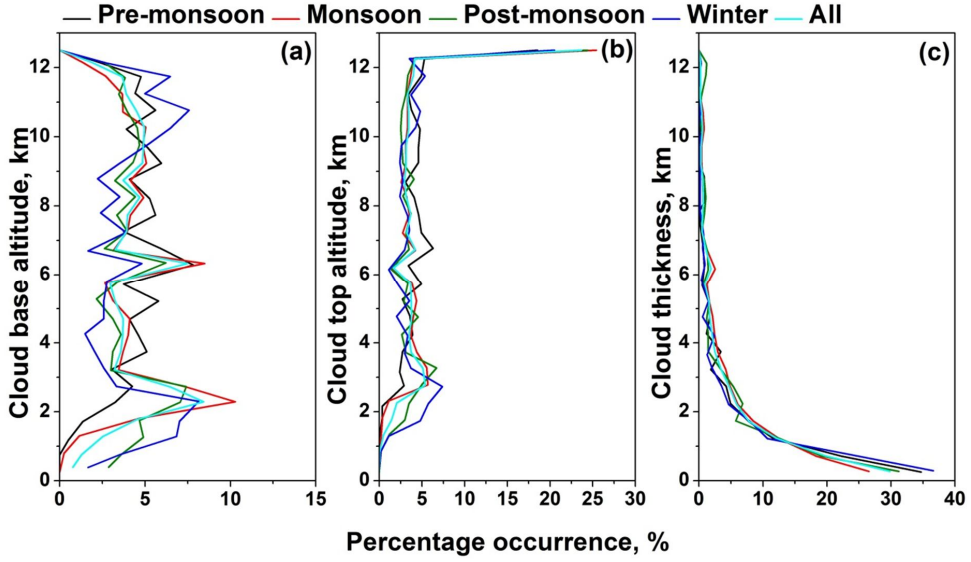

902

903 **Figure 8.** Percentage occurrence of the (a) cloud base altitude, (b) cloud top altitude and (c)

904 cloud thickness observed during different seasons over Gadanki. Altitude bin size is 500 m.

905

906

Atmos. Chem. Phys. Discuss., https://doi.org/10.5194/acp-2018-194
Manuscript under review for journal Atmos. Chem. Phys.
Discussion started: 5 April 2018

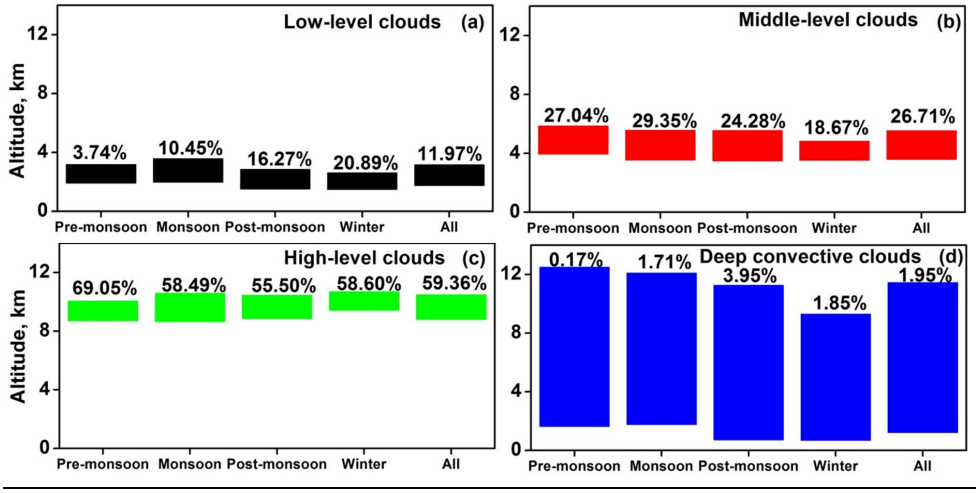

Figure 9. Mean vertical locations (base and top), cloud thicknesses and percentage occurrence of (a) low-level clouds, (b) middle-level clouds, (c) high-level clouds and (d) Deep convective clouds observed during different seasons.

Atmos. Chem. Phys. Discuss., https://doi.org/10.5194/acp-2018-194
Manuscript under review for journal Atmos. Chem. Phys.
Discussion started: 5 April 2018

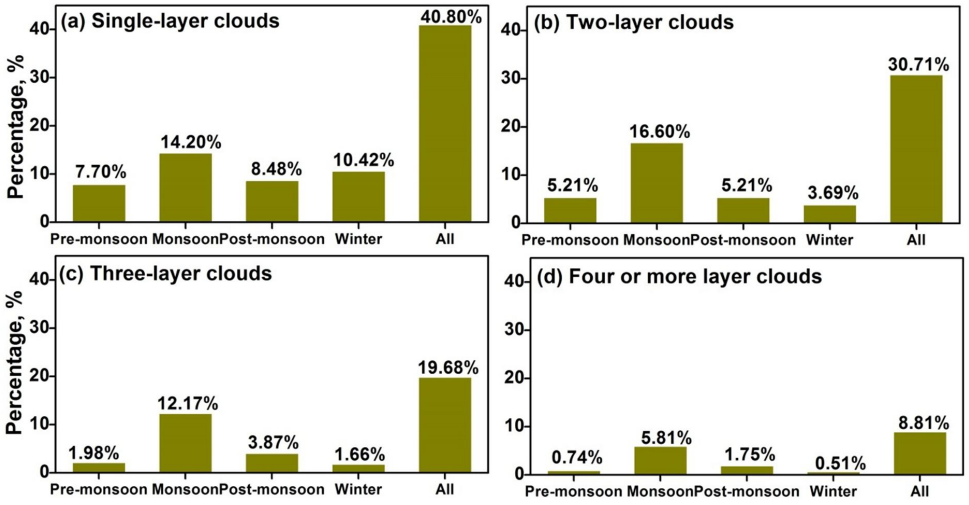

Figure 10. Percentage occurrence of (a) one-layer, (b) two-layer, (c) three-layer, and (d) four- or more- layer clouds observed during different seasons.

Atmos. Chem. Phys. Discuss., https://doi.org/10.5194/acp-2018-194
Manuscript under review for journal Atmos. Chem. Phys.
Discussion started: 5 April 2018

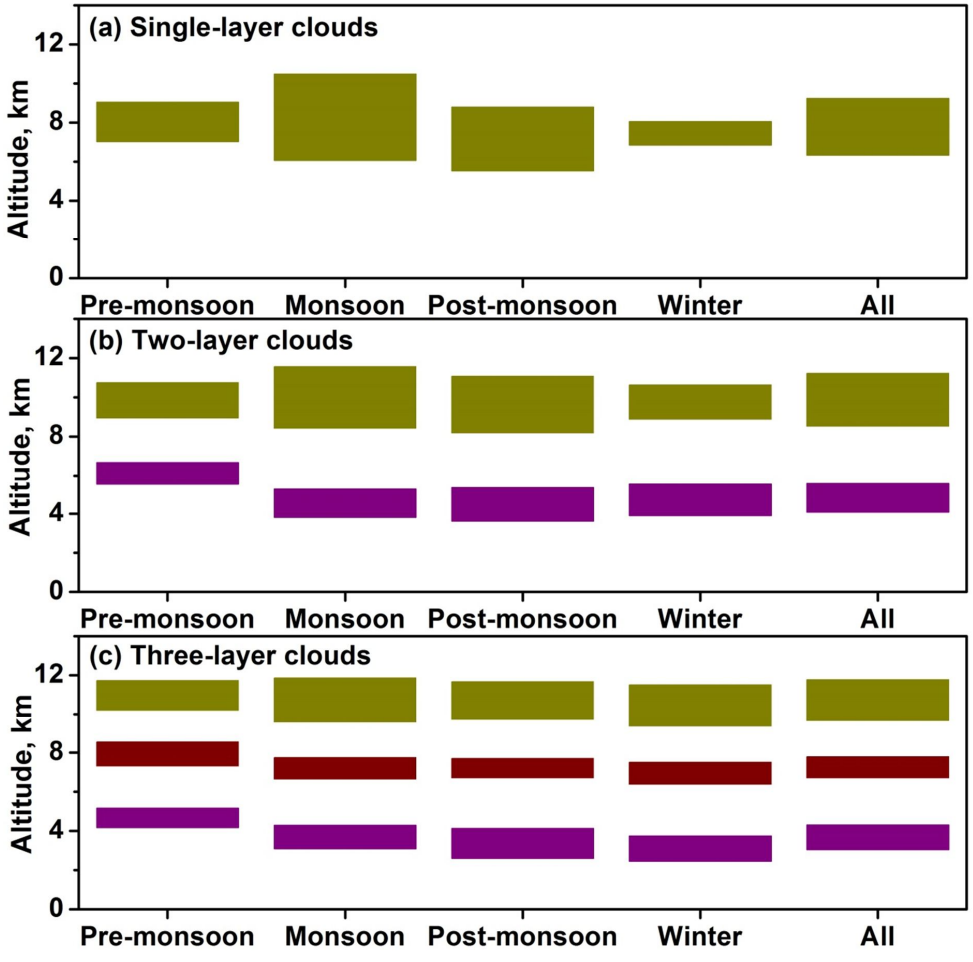

Figure 11. Mean vertical locations (base and top), cloud thicknesses of (a) one-layer clouds, (b) two-layer clouds, (c) three-layer clouds observed during different seasons.

Atmos. Chem. Phys. Discuss., https://doi.org/10.5194/acp-2018-194
Manuscript under review for journal Atmos. Chem. Phys.
Discussion started: 5 April 2018

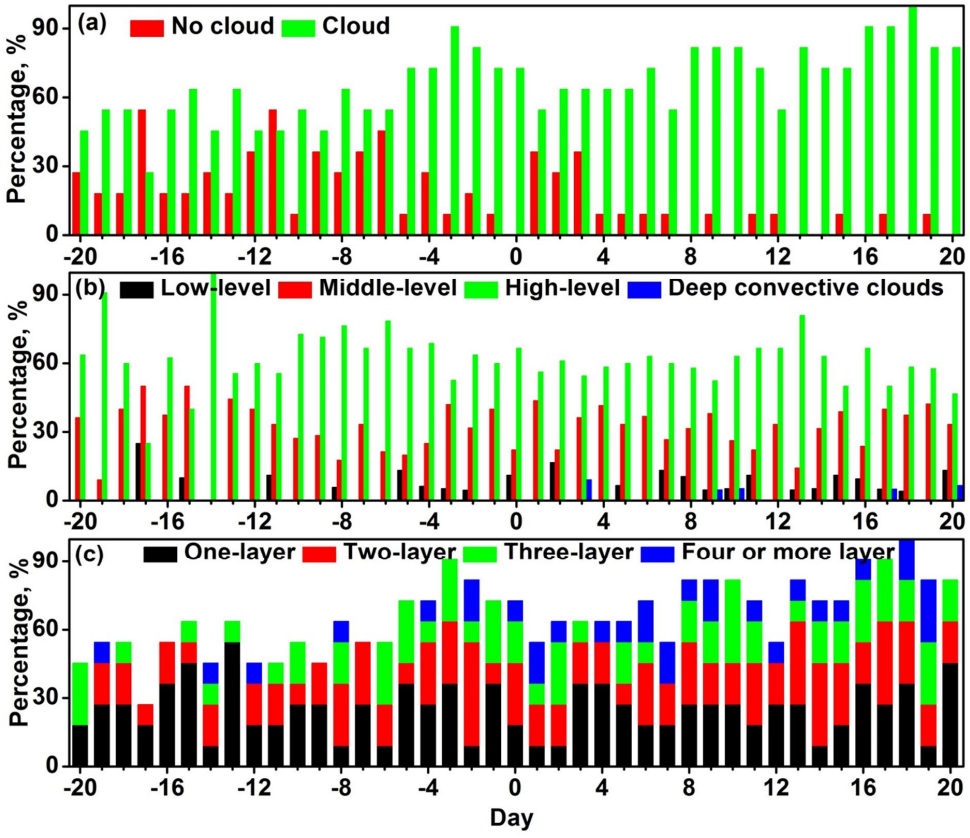

Figure 12. Composite (2006-2016) percentage occurrence of (a) clear and cloud conditions, (b) low-level, middle-level, high-level and deep convective cloud, and (c) one-, two-, three- and four or more- layer clouds observed with respect to the date of monsoon arrival over Gadanki location. Zero in x-axis indicates the date of monsoon arrival over Gadanki location.

Atmos. Chem. Phys. Discuss., https://doi.org/10.5194/acp-2018-194
Manuscript under review for journal Atmos. Chem. Phys.
Discussion started: 5 April 2018

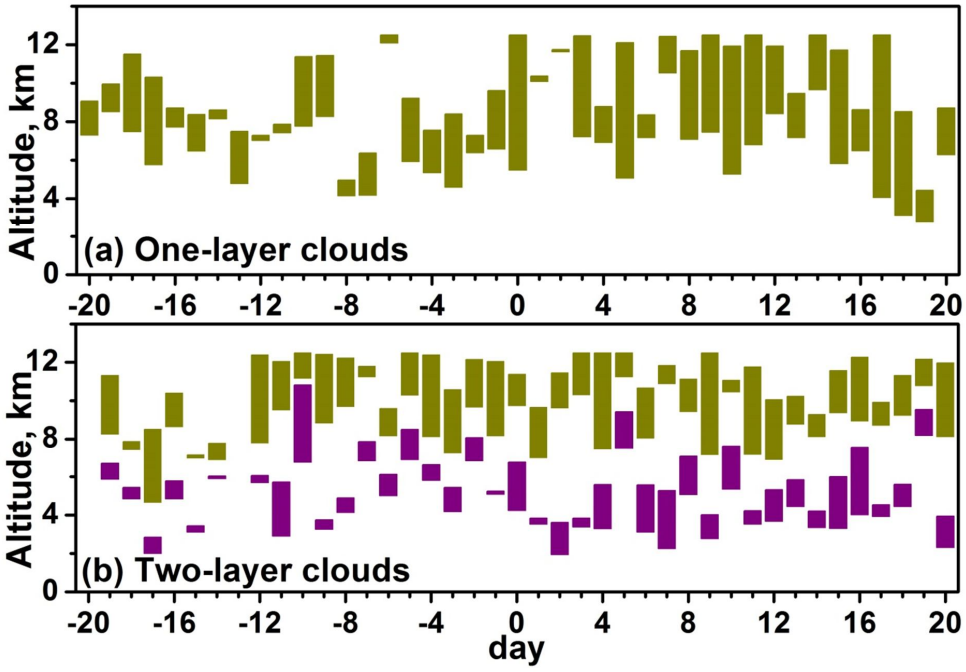

Figure 13. Composite (2006-2016) variations of mean vertical locations (base and top), thicknesses of one-layer clouds and two-layer clouds observed with respect to the date of monsoon arrival over Gadanki location. Zero in x-axis indicates the date of monsoon arrival over Gadanki location.

Atmos. Chem. Phys. Discuss., https://doi.org/10.5194/acp-2018-194
Manuscript under review for journal Atmos. Chem. Phys.
Discussion started: 5 April 2018

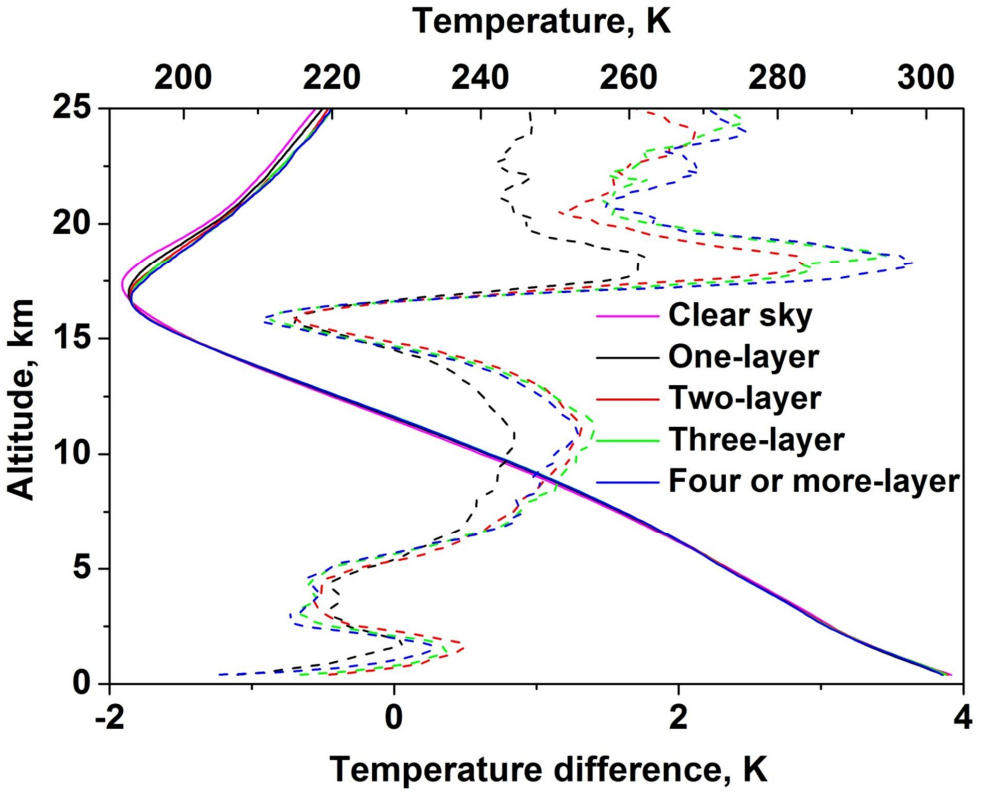

940

941 **Figure 14.** Composite (2006 – 2016) temperature profiles during clear sky, one-layer, two-
942 layer, three-layer and four or more-layer cloud occurrences. The respective temperature
943 difference profiles from clear sky conditions are shown with dash lines.

944

945

946

947

948

949

950

951